



HAL
open science

Expanding mechanistic models to represent purple phototrophic bacteria enriched cultures growing outdoors

Gabriel Capson-Tojo, Damien J Batstone, Tim Hülsen

► **To cite this version:**

Gabriel Capson-Tojo, Damien J Batstone, Tim Hülsen. Expanding mechanistic models to represent purple phototrophic bacteria enriched cultures growing outdoors. *Water Research*, 2023, 229, pp.119401. 10.1016/j.watres.2022.119401 . hal-03871919

HAL Id: hal-03871919

<https://hal.science/hal-03871919>

Submitted on 25 Nov 2022

HAL is a multi-disciplinary open access archive for the deposit and dissemination of scientific research documents, whether they are published or not. The documents may come from teaching and research institutions in France or abroad, or from public or private research centers.

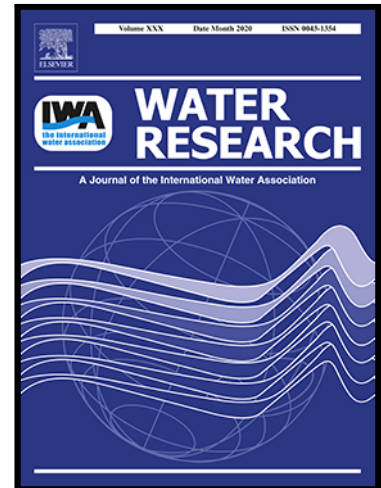
L'archive ouverte pluridisciplinaire **HAL**, est destinée au dépôt et à la diffusion de documents scientifiques de niveau recherche, publiés ou non, émanant des établissements d'enseignement et de recherche français ou étrangers, des laboratoires publics ou privés.

Journal Pre-proof

Expanding mechanistic models to represent purple phototrophic bacteria enriched cultures growing outdoors

Gabriel Capson-Tojo , Damien J. Batstone , Tim Hülsen

PII: S0043-1354(22)01346-X
DOI: <https://doi.org/10.1016/j.watres.2022.119401>
Reference: WR 119401



To appear in: *Water Research*

Received date: 14 June 2022
Revised date: 17 October 2022
Accepted date: 20 November 2022

Please cite this article as: Gabriel Capson-Tojo , Damien J. Batstone , Tim Hülsen , Expanding mechanistic models to represent purple phototrophic bacteria enriched cultures growing outdoors, *Water Research* (2022), doi: <https://doi.org/10.1016/j.watres.2022.119401>

This is a PDF file of an article that has undergone enhancements after acceptance, such as the addition of a cover page and metadata, and formatting for readability, but it is not yet the definitive version of record. This version will undergo additional copyediting, typesetting and review before it is published in its final form, but we are providing this version to give early visibility of the article. Please note that, during the production process, errors may be discovered which could affect the content, and all legal disclaimers that apply to the journal pertain.

© 2022 Elsevier Ltd. All rights reserved.

Highlights

- A model was developed to represent outdoors PPB mixed systems.
- Relevant clades, metabolic routes and environmental conditions were considered.
- The model included light and temperature dependence and aerobic conditions.
- The model was calibrated and validated using experimental pilot data.
- Simulations suggest optimal reactor design and working conditions/strategies.

Journal Pre-proof

Expanding mechanistic models to represent purple phototrophic bacteria enriched cultures growing outdoors

Gabriel Capson-Tojo ^{a,b,c}*, Damien J. Batstone ^a, Tim Hülsen ^a

^a Australian Centre for Water and Environmental Biotechnology, The University of Queensland, Brisbane, QLD, 4072, Australia

^b CRETUS, Department of Chemical Engineering, Universidade de Santiago de Compostela, 15782 Santiago de Compostela, Galicia, Spain

^c INRAE, Univ Montpellier, LBE, 102 Avenue des Etangs, 11100, Narbonne, France

* Corresponding author: tel. +34 606 23 14 95, e-mail: gabriel.capson-tojo@inrae.fr

Abstract

The economic feasibility of purple phototrophic bacteria (PPB) for resource recovery relies on using enriched-mixed cultures and sunlight. This work presents an extended Photo-Anaerobic Model (ePAnM), considering: (i) the diverse metabolic capabilities of PPB, (ii) microbial clades interacting with PPB, and (iii) varying environmental conditions. Key kinetic and stoichiometric parameters were either determined experimentally (with dedicated tests), calculated, or gathered from literature. The model was calibrated and validated using different datasets from an outdoors demonstration-scale reactor, as well as results from aerobic and anaerobic batch tests. The ePAnM was able to predict the concentrations of key compounds/components (*e.g.*, COD, volatile fatty acids, and nutrients), as well as microbial

communities (with anaerobic systems dominated by fermenters and PPB). The results underlined the importance of considering other microbial clades and varying environmental conditions. The model predicted a minimum hydraulic retention time of 0.5 d^{-1} . A maximum width of 10 cm in flat plate reactors should not be exceeded. Simulations showed the potential of a combined day-anaerobic/night-aerobic operational strategy to allow efficient continuous operation.

Keywords

Resource recovery; wastewater treatment; mechanistic modelling; purple phototrophic bacteria

Abbreviations and symbols

a	Peak irradiance during the zenith
ADM1	Anaerobic Digestion Model 1
ASRB	Autotrophic sulphate reducing bacteria
ALBAZOD	Algae, bacteria, zooplankton, and detritus mixture
AnMBR	Anaerobic membrane bioreactor
ASM	Activated Sludge Model
b	Zenith hour
BOM	Bureau of Meteorology
c	Parameter determining the bell width
CTMI	Cardinal temperature model with inflexion
COD	Chemical oxygen demand
DAF	Dissolved air flotation
DO	Dissolved oxygen

ePAnM	Extended Photo-Anaerobic Model
FIA	Flow injection analysis
FID	Flame ionisation detector
GC	Gas chromatography
HOB	Hydrogen-oxidizing bacteria
HRT	Hydraulic retention time
HSRB	Heterotrophic sulphate reducing bacteria
I	Light intensity
I_{ave}	Average light intensity in the growth media
I_{IN}	Limiting function for S_{IN}
I_{IP}	Limiting function for S_{IP}
I_{TAN}	Inhibition function for ammonia-N
I_{LI}	Inhibition function for suppression of heterotrophic metabolism of microalgae in the presence of light
I_L	Limiting function for light
I_{pH}	Inhibition function for pH
I_T	Inhibition function for temperature
IWA	International Water Association
K_{AC}	Half saturation constant for phototrophic SAC uptake by X_{PB}
K_L	Light intensity at which $k_m = 0.50 \cdot k_{opt}$
k_{La}	Volumetric mass transfer coefficient
K_{VFA}	Half saturation constant for phototrophic SVFA uptake by X_{PB}
K_S	Saturation constant
k_m	Uptake rate
k_M	Maximum specific uptake rate

$k_{M,ac}$	Maximum photoheterotrophic S_{AC} uptake rate for X_{PB}
$k_{M,vfa}$	Maximum photoheterotrophic S_{VFA} uptake rate for X_{PB}
k_{opt}	Maximal uptake rate
LED	Light-emitting diode
NIR	Near infrared
N_{XB}	N content in biomass
OD	Optical density
OLR	Organic loading rate
PAnM	Photo-Anaerobic Model
PBR	Photobioreactor
PCM1	Generalised Physicochemical Model No. 1
PHA	Polyhydroxyalkanoate
pH_{LL}	Lower inhibition term
pH_{UL}	Upper inhibition term
PPB	Purple phototrophic bacteria
P_{XB}	P content in biomass
R^2	Coefficient of determination
S_{AC}	Acetate
S_{H2}	Molecular hydrogen
S_I	Soluble inerts
S_{IC}	Inorganic carbon
S_{IN}	Inorganic nitrogen
S_{IP}	Inorganic phosphorus
S_O	Molecular oxygen
S_{ORG}	Soluble organics

S_S	Sulphide
S_{SO_4}	Sulphate
S_{VFA}	Non-acetate VFAs
SCP	Single-cell protein
SCOD	Soluble chemical oxygen demand
T_{max}	Temperature above which the growth is assumed to be zero
T_{min}	Temperature below which the growth is assumed to be zero
T_{opt}	Temperature corresponding to the maximal uptake rate
TCOD	Total chemical oxygen demand
TKN	Total Kjeldahl nitrogen
TN	Total nitrogen
TP	Total phosphorus
TS	Total solids
TSS	Total suspended solids
UV-VIS	Ultraviolet-visible
VIS	Visible
VFA	Volatile fatty acid
VS	Volatile solids
VSS	Volatile suspended solids
X_{Ac}	Acetogenic biomass
X_{Aer}	Aerobic heterotrophs biomass
X_{Alg}	Microalgae biomass
X_{ASRB}	ASRB biomass
X_C	Composites
X_H	Acidogenic biomass

X_{HSRB}	HSRB biomass
X_{I}	Inert solids
X_{PB}	PPB biomass
X_{Pred}	Aerobic predators

1. Introduction

Resource recovery is gaining importance in the wastewater treatment sector, which is moving away from the traditional “removal and disposal” approach. Biological upconcentration of materials and energy via assimilative and/or accumulative partitioning appears as a promising alternative to promote this transition, reducing the dissipative removal of organics and nitrogen while enabling phosphorus recovery (Batstone et al., 2015). For effective competition with traditional technologies, these novel processes must not only provide an effective wastewater treatment, but also generate high value-added products (*e.g.*, single-cell protein (SCP), fertilisers, hydrogen, polyhydroxyalkanoates (PHA) or pigments) than can balance their higher costs, which is particularly relevant for capital intense photobioreactors (PBRs).

Phototrophic mediators have been gaining attention for resource recovery due to their ability to use light as energy source for assimilative (*vs.* oxidative) pollutant removal. Microalgae have been extensively researched for both secondary and tertiary treatment, with promising results in terms of nutrient (*i.e.*, N and P) removal and recovery efficiencies (Robles et al., 2020b). Nevertheless, if there is chemical oxygen demand (COD) in wastewaters, algae-based processes result in the growth of non-phototrophic flanking organisms, generating a mixed community commonly referred to as ALBAZOD (algae, bacteria, zooplankton, and detritus mixture). This reduces the COD and N recovery efficiencies (Muñoz and Guieysse, 2006), and frequently results in predation by aerobic grazers (Day et al., 2017). Purple phototrophic

bacteria (PPB) have appeared in the last decade as a promising alternative, as they are able to grow photoheterotrophically when illuminated with near infrared (NIR) light under anaerobic conditions, assimilating simultaneously COD and nutrients (Hülßen et al., 2014).

PPB, consisting mostly of purple sulphur and purple non-sulphur bacteria, perform anoxygenic photosynthesis, using light as energy source (mostly in the NIR spectra thanks to the presence of bacteriochlorophylls), and a range of electron donors other than water. Under anaerobic illuminated conditions, PPB can grow autotrophically, with inorganic compounds as donors (*e.g.*, H_2 , H_2S , S_0 , $\text{S}_2\text{O}_3^{2-}$ or Fe^{2+}) or via photoheterotrophy, using organic compounds such as acetate, propionate, butyrate, or malate as electron donors. PPB can also grow in the dark, either anaerobically via fermentation or aerobically via respiration if oxygen is present (Zeilstra-Ryalls et al., 1998). The main competitive advantage of PPB under non-sterile conditions is their ability to grow photoheterotrophically. Effective and competitive growth is further facilitated by the uptake of electron donors with relatively low carbon oxidation state (*e.g.*, acetate) (Hülßen et al., 2018). Under anaerobic illuminated conditions, their high photon utilisation efficiency (*i.e.*, 6-8% *vs.* < 5% for microalgae (Posten and Schaub, 2009)) and their capability to recycle electrons (cyclic electron flow in anoxygenic photosynthesis) enable biomass yields around $1.0 \text{ g COD}_{\text{biomass}} \cdot \text{g COD}_{\text{removed}}^{-1}$ (*vs.* 0.5 and < $0.2 \text{ g COD} \cdot \text{g COD}_{\text{removed}}^{-1}$ for aerobic heterotrophs and anaerobic fermenters (Batstone et al., 2002; Henze et al., 2002)). Their capability of disposing excess electrons to maintain cell homeostasis by diverse mechanisms (*e.g.*, CO_2 refixation via the Calvin cycle, PHA accumulation or hydrogen production via nitrogenase activity) allows them to regenerate reduced cofactors and to grow at yields over $1.0 \text{ g C} \cdot \text{g C}^{-1}$, depending of the oxidation state of the carbon donor (Madigan et al., 2011).

PPB have been effectively applied for the treatment of a range of wastewaters, including domestic (Hülßen et al., 2016b), swine (Kim et al., 2004), poultry processing, red meat, dairy

(Hülßen et al., 2018), and sugar refinery wastewaters (Yetis et al., 2000). The pollutant removal occurs due to microbial uptake, which implies that adequate COD:N:P ratios in the wastewater are crucial to achieve complete nutrient removal. Optimal COD:N:P uptake ratios around 100:6-10:1-2 have been reported (Lu et al., 2019; Puyol et al., 2017). Median COD, N and P removal efficiencies under illuminated-anaerobic conditions of 76%, 53% and 58% have been recently reported (Capson-Tojo et al., 2020a). The same review pointed out that most studies to date have been carried out under axenic conditions, using pure cultures and under artificial illumination. Although these conditions are necessary to develop a proof-of-concept and for research purposes, outdoor studies, using mixed PPB cultures under non-sterile conditions, are required to determine the actual performance under varying environmental conditions.

Bioprocess modelling is a useful tool for the design, study, optimisation, control, and system analysis of wastewater treatment processes. The IWA Activated Sludge models (ASM1-3) and the IWA Anaerobic Digestion model no.1 (ADM1) or their commercial analogues are the most widely applied models for activated sludge and anaerobic digestion processes (Batstone et al., 2002; Henze et al., 2000). These models have been an invaluable tool for academic and industrial applications, and novel technologies such as PPB-based recovery processes would benefit immensely from mechanistic models able to represent accurately these systems. To date, mathematical models representing metabolic processes on a cellular level (*e.g.*, electron transport chain reactions or metabolic network modelling) are available for single applications with individual PPB species (Hädicke et al., 2011; Klamt et al., 2008). Nevertheless, these models are not practical for mixed communities. Instead, mechanistic biochemical process modelling can be considered as a simpler option to represent functional groups on a community level (Batstone et al., 2019). Most mechanistic models for PPB have been directed towards the prediction of hydrogen production via PPB (Akbari and Mahmoodzadeh Vaziri,

2017; Gadhamshetty et al., 2008; Obeid et al., 2009; Zhang et al., 2015), and so far, only one mechanistic model exists to represent wastewater treatment and nutrient recovery by PPB: the Photo-anaerobic model (PANM) developed by Puyol et al. (2017). This model (with PPB as single biomass component) accurately represented laboratory-scale performances in controlled environments (*e.g.*, under constant artificial illumination and temperature, and fed with synthetic media). Nevertheless, mechanistic models applicable to future full-scale PPB-based processes must consider the complex nature of the waste streams to be treated, the varying environmental conditions that the reactors will be exposed to (*e.g.*, changing temperatures and light intensities, day-night cycles, *etc.*), and potential synergies and competitions with other microorganisms (non-axenic conditions must be assumed when treating waste streams).

Such models do exist for other phototrophic organisms (*i.e.*, microalgae), and they can serve as building body for the development of PPB models. Mixed-culture comprehensive mechanistic models for microalgae have been developed, particularly to consider the interactions between microalgae and heterotrophic bacteria (Casagli et al., 2021; Solimeno et al., 2019; Solimeno and García, 2017). As they represent a convenient compromise between prediction capabilities and simplicity, biochemical mechanistic models are the most commonly applied models (Darvehei et al., 2018; Shoener et al., 2019). Nevertheless, dedicated models have also been developed to consider other relevant factors, such as fluid heterogeneity in PBRs (*e.g.*, via computational fluid dynamics (Ranganathan et al., 2022)), outdoors solar irradiance and light distribution throughout the culture (Acién Fernández et al., 1997; Béchet et al., 2013), or temperature prediction in the reactors (*e.g.*, heat transfer modelling (Todisco et al., 2022)). Although none of these approaches has been applied for PPB systems, this technology could clearly benefit from them.

For an economically feasible application of PPB for resource recovery from wastewater,

outdoors operation is required, using sunlight as energy source (Capson-Tojo et al., 2020a). The feasibility of outdoors PPB growth in bioreactors for resource recovery from wastewater has been confirmed recently. Using outdoors flat plate PBRs (80-100 L of total volume) working in batch, removal efficiencies for soluble COD (SCOD), total nitrogen (TN), and total phosphorus (TP) of 20-60%, 2-30%, and 3-40% were reported, respectively (from poultry-processing and piggery wastewater). Biomass productivities up to $18 \text{ g}\cdot\text{m}^{-2}\cdot\text{d}^{-1}$ were achieved in those experiments, with consistent crude protein contents of 65% (Hülßen et al., 2022a). The potential of this technology and the current stage of technological advancement call for the development of a mechanistic model able to assist with reactor design, operational strategy assessment, troubleshooting, and decision-making.

This article presents a detailed mechanistic model applicable for mixed PPB cultures grown outdoors, as an extension of the PAnM model (ePAnM). Relevant microbial clades interacting with PPB have been included (*e.g.*, aerobic heterotrophs, acidogenic and acetogenic fermenters, aerobic predators, heterotrophic and autotrophic sulphate reducing bacteria (HSRB and ASRB) and microalgae). PPB metabolism has been extended, including fermentative, aerobic chemoheterotrophic, and photoautotrophic growth. Inhibitory effects have been added, including the effect of oxygen or acid/basic pH values on phototrophic metabolism (Capson-Tojo et al., 2021, 2020a). To do so, main physico-chemical processes have also been considered (*e.g.*, speciation and chemical equilibria of main species, or gas-liquid mass transfer). The impact of varying temperatures and light intensities on PPB growth rates, as well as light attenuation through the culture, have also been included (Capson-Tojo et al., 2022). The model was calibrated and validated using data from different operational periods from a demonstration-scale flat plate reactor (Hülßen et al., 2022b), and with batch tests.

2. Material and methods

This section focuses on model structure and development. Accurate descriptions of the reactor operation, analytical methods, and general data analysis (*i.e.*, parameter calibration, biomass yields calculation, estimation of daily light distributions from average solar exposures, and estimation of kinetic parameters and inhibitory constants) can be found in appendices to the article.

2.1. Model description and Photo-Anaerobic Model extension

The ePAnM was developed to be compatible with the IWA ADM1 and ASM series, following the IWA benchmark (Batstone et al., 2002; Henze et al., 2000; Jeppsson et al., 2006). Organics are expressed in $\text{g COD}\cdot\text{m}^{-3}$, nutrients are expressed in $\text{g N}\cdot\text{m}^{-3}$ or $\text{g P}\cdot\text{m}^{-3}$, sulphur as $\text{g S}\cdot\text{m}^{-3}$, and inorganic carbon in $\text{kmol C}\cdot\text{m}^{-3}$. Monod kinetics were chosen as rate equations for biological uptake processes, and first order processes for hydrolysis and decay. If not specified otherwise, Monod inhibition functions were used in limiting or inhibitory expressions.

Anaerobically, both the photoheterotrophic and photoautotrophic capabilities of PPB were considered, using VFAs (*i.e.*, acetic acid or other VFA) and molecular hydrogen or hydrogen sulphide as electron donors, respectively. H_2S (and thus S) metabolism was added due to its relevance when sulphate is present, such it is the case in urban wastewater streams or some saline effluents (Durán et al., 2020; Hülsen et al., 2019). As PPB are not able to reduce sulphates, two other bacterial clades capable of doing so (*i.e.*, HSRB and ASRB) were added, based on Durán et al. (2020). Known intermediate S species such as thiosulphate or elemental sulphur have been omitted for simplicity (Egger et al., 2020). The fermentative capabilities of PPB were also included. In addition, both acidogenic and acetogenic bacterial clades were added, as their faster fermentation rates compared to PPB ensure their presence (*e.g.* uptake rates of $15\text{-}30\text{ d}^{-1}$ for fermenters *vs.* 0.074 d^{-1} for PPB) (Batstone et al., 2002; Puyol et al.,

2017). The presence of fermentative bacteria in PPB-based processes treating complex wastewater has been confirmed (Alloul et al., 2021; Hülsen et al., 2022a, 2018, 2016b).

The aerobic capabilities of PPB were also included, using VFAs and organics as carbon and electron sources. Aerobic heterotrophic biomass was included as main PPB competitors under the presence of oxygen (Capson-Tojo et al., 2021; Izu et al., 2001). Aerobic conditions were included for two main reasons: (i) the strong inhibition of the phototrophic capabilities of PPB by oxygen, and (ii) the potential relevance of alternate anaerobic/aerobic processes in PPB technology (Hülsen et al., 2022b). Aerobic predators (grazers) were included due to experimental evidence of their relevance under continuous aeration (Capson-Tojo et al., 2021).

Microalgae were included in the model to consider potential phototrophic competitors, as well as combined processes where both PPB and algae could coexist (Hülsen et al., 2022a), a system that arises when providing unfiltered (sun)light (Hülsen et al., 2022a). A simplified version of the model presented in Wagner et al. (2016) was implemented, considering directly the processes responsible for microalgal growth. To separate microalgae from PPB growth, the model considered two different light inputs, one at visible (VIS) wavelengths (400-700 nm; allowing algae growth) and another at NIR wavelengths (>700 nm; preferable for PPB).

The single form of electron disposal considered in the ePAnM under anaerobic conditions is CO₂ refixation via the Calvin Cycle. This is because most wastewaters have an excess of nutrients, which excludes the occurrence of other electron disposal mechanisms, such as hydrogen production (by-product of N fixation) or PHA accumulation (modification of standard anabolism) (Capson-Tojo et al., 2020a; Hülsen et al., 2016b). No Poly-P accumulation nor any other form of P storage were considered. Nitrification and denitrification processes were not considered, as they are only relevant under predominantly aerobic conditions and long sludge retention times. Thus, the model assumes that N and P

removals occur due to assimilation.

The PAnM (Puyol et al., 2017) considers PPB as single biomass, including their fermentative and phototrophic capabilities and assuming constant environmental conditions. The ePAnM considers many other biomass components, processes, inhibitory factors, and varying environmental factors. All are described below.

2.1.1. Components, processes, and inhibitory factors

The ePAnM consists of 21 components (plus 7 to consider ionic equilibria and CO₂ desorption), 30 biochemical processes, and 8 inhibition factors. The corresponding Petersen matrix is shown in Table 1. The soluble components considered in the ePAnM are: non-acetate VFAs (S_{VFA}), acetate (S_{AC}), inorganic carbon (S_{IC}), molecular hydrogen (S_{H_2}), molecular oxygen (S_O), inorganic nitrogen (S_{IN}), inorganic phosphorus (S_{IP}), soluble organics (S_{ORG}), soluble inerts (S_I), sulphate (S_{SO_4}) and sulphides (S_S). Regarding particulate components, those are: PPB biomass (X_{PB}), aerobic heterotrophs biomass (X_{Aer}), acidogenic biomass (X_H), acetogenic biomass (X_{Ac}), aerobic predators (X_{Pred}), HSRB biomass (X_{HSRB}), ASRB biomass (X_{ASRB}), microalgae biomass (X_{Alg}), composites (X_C), and inert solids (X_I). The model includes the following processes: hydrolysis (1; in contrast with the PAnM, separated from fermentation via the inclusion of S_{ORG} and fermentative clades); photoheterotrophic uptake by X_{PB} of S_{VFA} and S_{AC} (2-3); fermentation by X_{PB} (4-5); aerobic uptake of S_{AC} , S_{VFA} and S_{ORG} by X_{PB} (6-8); aerobic uptake of S_{AC} , S_{VFA} and S_{ORG} by X_{Aer} (9-11); S_{ORG} uptake by X_H (12); S_{VFA} uptake by X_{Ac} (13); autotrophic uptake of S_{H_2} by X_{PB} (14); uptake by X_{Pred} (15-16); S_{AC} and S_{VFA} uptake by X_{HSRB} (17-18); autotrophic uptake of S_{H_2} by X_{ASRB} (19); autotrophic uptake of S_S by X_{PB} (20); autotrophic and heterotrophic uptake by X_{Alg} (21-22); and biomass decay (23-30).

Regarding inhibition factors, Monod inhibition functions as limiting expressions were considered for S_{IN} (I_{IN}) and S_{IP} (I_{IP}). Inhibitions due to ammonia-N (I_{TAN}), oxygen (I_O) or light

were (I_L) were also considered (see Table 1). I_{TAN} inhibition was included in the model for PPB uptake processes, according to Puyol et al. (2020, 2017). Considering the ammonia-N levels that are commonly reached in wastewater streams, and according to previous literature, ammonia-N inhibition was not considered for any other microbial clade (Batstone et al., 2002; Durán et al., 2020; Henze et al., 2000; Wágner et al., 2016). The presence of oxygen was considered inhibitory for all anaerobic processes (*i.e.*, fermentation, and photoheterotrophy and photoautotrophy by PPB) (Batstone et al., 2002; Capson-Tojo et al., 2021; Durán et al., 2020). An inhibition term was also included to represent the suppression of the chemoheterotrophic metabolism of microalgae in the presence of light (I_{LI}) (Wágner et al., 2016). The inhibitory terms associated to light (I_L), pH (I_{pH}) and temperature (I_T) are discussed in Section 2.1.2.

When available, process stoichiometry, kinetic expressions, initial kinetic parameters, and stoichiometric coefficients were obtained from the literature. The ASM1 was used as base for aerobic growth (Henze et al., 2000), and the ADM1 for acidogenic and acetogenic processes (Batstone et al., 2002). The work of Durán et al. (2020) was used as base to represent non-PPB S-related processes. Different studies were used for PPB-related processes (Capson-Tojo et al., 2022, 2021; Egger et al., 2020; Puyol et al., 2020, 2017). Predation was modelled according to Ni et al. (2011) and Moussa et al. (2005), and microalgae growth according to Wágner et al. (2016). When no information was available, parameters were calculated theoretically or determined experimentally (see coming sections). Continuity equations were applied over COD, C, N, P and S for stoichiometric calculations. S_{ORG} was assumed to consist on a mixture of sugars, aminoacids, and fatty acids in equal proportions (compositions from Batstone et al. (2002)). S_{VFA} was assumed to consist of 50% propionate and 50% butyrate. As in the ADM1, S_{IN} and S_{IP} stoichiometry was determined by N and P balances over each process, respectively.

Other than initial values of state variables and the corresponding numbers from the influent in continuous systems, the model uses as inputs: (i) the concentrations of species in equilibrium with acids or bases included in the pH model (*i.e.*, anionic VFA conjugates, bicarbonate, free ammonia, biphosphate and bisulfide), (ii) the temperature in the reactor, (iii) the influent flow rate ($L \cdot d^{-1}$), (iv) the incident light ($W \cdot m^{-2}$), (v) the VIS fraction in incident light, and (vi) the NIR fraction in incident light. The hydraulic retention time (HRT), the volumetric mass transfer coefficient (k_{La}), and the concentrations of metallic cations/anions in the reactor (assumed as constant (Batstone et al., 2002)) are also values that must be specified. CO_2 liquid-gas transfer was also included due to its influence on the pH (as in the ADM1), assuming atmospheric pressure on the gas/liquid interface (Batstone et al., 2002).

The corresponding stoichiometric balance files and MATLAB codes can be found in the supplementary material and GitHub (<https://github.com/GabrielCapson/Extended-PAnM.git>).

2.1.2. Changing environmental conditions: influence of light intensity, temperature, and pH

The effect of varying light intensities and temperatures on phototrophic uptake rates (for both microalgae and PPB) was represented using uncoupled models (Béchet et al., 2013). The Steele's equation was used to represent the influence of light intensity on uptake rates of algae (Béchet et al., 2013; Ruiz-Martínez et al., 2016; Wágner et al., 2016). For PPB, a Monod inhibition function was used (no photoinhibition was observed in common illumination ranges) (Capson-Tojo et al., 2022; Puyol et al., 2017). The general expression is as follows:

$$k_m = k_{opt} \cdot I_L(I) = k_{opt} \cdot \frac{I}{I+K_L} \quad (1)$$

Where k_m (d^{-1}) is the uptake rate, I is the light intensity ($W \cdot m^{-2}$), k_{opt} (d^{-1}) is the maximal uptake rate and K_L is light intensity at which $k_m = 0.50 * k_{opt}$ ($W \cdot m^{-2}$).

Light attenuation through the culture was modelled using the Lambert-Beer equation, applying an empirical power relationship to model the effect of biomass concentration on the attenuation coefficients (Capson-Tojo et al., 2022). The average light intensity in the growth media (I_{ave}) was used as input for biological growth (Béchet et al., 2013).

The influence of temperature on uptake rates of phototrophic organisms was modelled using the cardinal temperature model with inflexion (CTMI), which has been successfully applied previously for indoors and outdoors microalgal cultures (Bernard and Rémond, 2012; Ruiz-Martínez et al., 2016). The CTMI is of the form:

$$k_m \begin{cases} 0 & \text{if } T < T_{min} \\ k_{opt} \cdot I_T(T) & \text{for } T_{min} < T < T_{max} \\ 0 & \text{if } T > T_{max} \end{cases} \quad (2)$$

$$I_T(T) = \frac{(T - T_{max}) \cdot (T - T_{min})^2}{(T_{opt} - T_{min}) \cdot [(T_{opt} - T_{min}) \cdot (T - T_{opt}) - (T_{opt} - T_{max}) \cdot (T_{opt} + T_{min} - 2 \cdot T)]} \quad (3)$$

T_{min} (°C), T_{max} (°C) are the temperatures below and above which the growth is assumed to be zero. T_{opt} (°C) is the temperature corresponding to the maximal uptake rate k_{opt} (d⁻¹).

The influence of temperature on the uptake and decay rates of non-phototrophic microbial clades was modelled using the Arrhenius equation, via interpolation of kinetic parameters (Henze et al., 2000). Values of aerobic growth and decay rates were collected from Henze et al. (2000). Values of Arrhenius factors for hydrolysis and uptake and decay rates for fermenters (*i.e.*, acidogens and acetogens), HSRB, and ASRB were taken from Durán et al. (2020).

The pH was modelled via charge balance, as in the ADM1 (Batstone et al., 2002), but including also the $H_2PO_4^-/HPO_4^{2-}$ and HS^-/S^{2-} acid-base pairs. Due to its relevance as inhibitor and for correct pH calculations, non-ideal corrections were applied to calculate the

concentration of free ammonia nitrogen, as in Capson-Tojo et al. (2020b). The effect of temperature on equilibrium constants was considered via the van't Hoff equation. The effect of pH over uptake rates was modelled according to an empirical lower inhibition function (Batstone et al., 2002):

$$I_{pH}(pH) = \begin{cases} 1 & \text{if } pH > pH_{UL} \\ e^{-3 \cdot \left(\frac{pH - pH_{UL}}{pH_{UL} - pH_{LL}} \right)^2} & \text{if } pH < pH_{UL} \end{cases} \quad (4)$$

Where pH_{LL} and pH_{UL} are the lower and upper inhibition terms, *i.e.*, the values where inhibition is complete and where there is no inhibition, respectively.

Inhibition due to low pH was only considered for PPB, HSBR and ASBR, according to previous recommendations and results (Capson-Tojo et al., 2020a; Durán et al., 2020). The values of the respective limits can be found in Table S1, together with the stoichiometric and kinetic parameters used. pH inhibition for aerobic heterotrophs and acidogenic/acetogenic fermenters was not included due to their known robustness to relatively wide pH ranges, far from the values that are expected in PPB-dominated systems. Upper inhibition limits could be added if deemed necessarily by using an empirical upper and lower inhibition function (Batstone et al., 2002).

A description of how the required batch tests were carried out can be found in Appendix A.

2.1.3. Model limitations and other relevant assumptions

Despite considering the growth of aerobic heterotrophs (and the potential presence of oxygen), nitrification and denitrification processes have been omitted. This is because the reactors are expected to be operated with excess organic carbon, and generally oxygen limited conditions (Capson-Tojo et al., 2021). Therefore, the concentrations of nitrates/nitrites are expected to be negligible in PPB-dominated systems (also due to short sludge retention

times). When treating streams rich in nitrogen oxides, denitrification/nitrification processes could be incorporated into the model, as in the ASM series (Henze et al., 2000). Uptake of nitrates and nitrites by microalgae has also been omitted, considering only ammonia-N as N source for algae growth.

Most systems for outdoors PPB growth are expected to be open to the atmosphere (*i.e.*, open PBRs or ponds). Nevertheless, the generation of gases other than CO₂ has not been considered. Hydrogen production might occur to some extent when treating effluents limited in NH₄⁺-N, but even in this situation, H₂ will be rapidly consumed by PPB if light is available (Capson-Tojo et al., 2020a). In addition, hydrogen production by PPB is not included in the model, as most potential waste streams have excess nutrients (Hülßen et al., 2018, 2016b). The production of methane has also been omitted, as the HRTs and sludge retention times that are commonly applied in PPB-based reactors are much lower than those in anaerobic digestion systems, causing washout of slow-growing methanogens. NH₃ stripping is excluded for the same reasons as in the ADM1 (*i.e.*, solubility is sufficiently high at the < 5,000 mg N·L⁻¹ range). The formation of precipitates is not considered in the ePAnM either, but could be included as in the IWA Generalised Physicochemical Model No. 1 (PCM1) (Batstone, 2021).

Extreme climates may need further corrections to consider the influence of temperature on uptake and decay rates for non-phototrophic clades. As an interpolation, the Arrhenius coefficients are most accurate between the temperature range that has been used for their calculation. As example, the coefficients from Durán et al. (2020) were determined via dynamic calibration with experimental data from an anaerobic membrane bioreactor (AnMBR) working between 14 and 33 °C. Therefore, the application of those coefficients out of this range might lead to over/underestimations of the uptake rates. In addition, microbial shifts due to adaptation to different temperatures have not been considered. Re-calibration

might be needed in this case.

The current model is not applicable to nutrient-limited streams where hydrogen production or PHA accumulation will occur to relevant extents. These processes can be added easily, as readily models representing both PHA accumulation (Henze et al., 2000) and hydrogen production via photofermentation already exist (Akbari and Mahmoodzadeh Vaziri, 2017; Gadhamshetty et al., 2008; Obeid et al., 2009; Zhang et al., 2015).

The photoheterotrophic uptake of sugars or alcohols by PPB is much slower than the fermentation kinetics of these organic compounds by acidogenic/acetogenic clades. Therefore, the uptake of sugars/alcohols via photoheterotrophy has not been considered in the model, as the occurrence of this process is expected to be minimal in enriched cultures. If needed, the concentration of these compounds could be lumped with that of S_{VFA} , as presented in the PAnM.

The presence of hydrogen-oxidizing bacteria (HOB) has been omitted for three main reasons: (i) they will only be present when hydrogen and oxygen are available simultaneously under non-illuminated conditions (situation not likely to occur); (ii) microbial analysis have shown that HOB are not present in PPB systems in significant proportions (Hülßen et al., 2022b, 2018, 2016b); (iii) hydrogen transfer into the gas phase is not considered in the model, so significant COD losses via this route are not accounted for.

2.2. Model calibration and validation using data from a demonstration-scale outdoors flat plate photobioreactor

The ePAnM was calibrated using data from a demonstration-scale PBR treating fermented poultry-processing wastewater outdoors (see Figure S1 for a simplified schematic of the plant) (Hülßen et al., 2022b). These data were chosen because they are representative of outdoors upscaled systems treating complex waste matrixes under varying environmental conditions (temperatures of 9.2-25 °C and peak daily solar irradiances of 325-788 $W \cdot m^{-2}$).

Therefore, this dataset was ideal to assess the accuracy of the ePanM to represent outdoor PPB systems. Data from daily cycle studies (samples every 2-4 h during over 24 h) was used for calibration to ensure an accurate representation of the daily fluctuations occurring in the plant. The description of the demonstration-scale PBR and its operation can be found in Appendices B and C. Appendix D describes the processes followed for parameter calibration and uncertainty analysis.

Data from a different operational period from the PBR was used for validation, as well as results from different batch tests under both anaerobic and aerobic conditions. The description of the operational conditions of the PBR and the batch tests can be found in Appendix C, and the characteristics of the treated wastewater in Table S2.

2.3. Simulating different scenarios: optimal operational conditions and day-anaerobic/night-aerobic continuous operation

The resulting model was used to simulate scenarios to estimate optimal operational conditions (*i.e.*, HRT) and design parameters (*i.e.*, reactor width). In addition, a potential scenario where a continuous-outdoors process can be maintained by combining anaerobic-photosynthetic growth during daytime and aerobic-chemoheterotrophic growth during night hours was simulated. The precise conditions assumed for each simulation are described in Appendix E.

3. Results and discussion

3.1. Parameter estimation and model calibration

3.1.1. Estimation of kinetic parameters at different temperatures

The specific acetate uptake rates corresponding to the experiments at different temperatures are shown in Figure 1, together with the resulting CTMI curve. The corresponding COD consumption/production curves can be found in Figure S2.

The selected model was able to accurately describe the effect of temperature on the acetate

uptake rates by PPB (R^2 of 0.97). The resulting maximum k_M ($2.68 \text{ g COD} \cdot \text{g COD}^{-1} \cdot \text{d}^{-1}$) is in agreement with previous reported values (Capson-Tojo et al., 2021; Puyol et al., 2017), which further confirms the validity of the results. The resulting temperature parameters given by the CTMI were $8.41 \text{ }^\circ\text{C}$ for T_{\min} , $30.2 \text{ }^\circ\text{C}$ for T_{opt} , and $52.0 \text{ }^\circ\text{C}$ for T_{\max} . An optimal growth temperature around $30 \text{ }^\circ\text{C}$ is common for bacteria present in mesophilic environments (Batstone et al., 2002; Henze et al., 2000). Nevertheless, the wide range between the minimum and maximum values for the obtained CTMI and the high value of T_{\max} is far less common (see Bernard and Rémond (2012) for examples for microalgae). Indeed, previous studies have shown efficient operation of PPB reactors at peak temperatures over $50 \text{ }^\circ\text{C}$ (Hülse et al., 2022b, 2022a). Similarly, studies at low temperatures have proven that PPB can efficiently treat wastewater even at temperatures below the T_{\min} reported here, although at lower uptake rates (Dalaei et al., 2019; Hülse et al., 2016a). As explained previously, adaptation of microbes to extreme environments has not been considered in this work, and the provided parameters must be recalibrated when working under conditions far from the ones applied here (as for mesophilic and thermophilic temperatures ranges in the ADM1).

Despite the acute nature of the tests performed (without allowing for microbial adaptation), the obtained results underline the remarkable resilience of PPB to temperature changes, with uptake rates practically unchanged between 20 to $40 \text{ }^\circ\text{C}$, and showing a wide survival range.

3.1.2. Model calibration using pilot data

To account for diurnal and nocturnal variations, data from a daily cycle study carried out in the demonstration-scale PBR was used for model calibration. Table 2 shows the resulting values of the kinetic parameters related to PPB phototrophic uptake and biomass compositions, which were calibrated to fit the experimental results (*i.e.*, concentrations of S_{AC} , S_{VFA} , S_{IN} , and S_{IP}). The corresponding plots, including modelled and experimental data, are shown in Figure 2, as well as the 95% confidence intervals. The complete parameter set

can be found in Table S1.

The calibrated model was able to predict the dynamics of both organic matter and nutrients, maintaining reasonable confidence intervals. The obtained parameters were well in line with those previously reported in the literature (see Table 2; (Capson-Tojo et al., 2022; Puyol et al., 2017)), although the k_M values were slightly higher than those presented in the PAnM. The confidence intervals of $k_{M,ac}$ were mostly within 95% confidence regions (Figure S3), further confirming the applicability of the parameters and their importance for accurate predictions. Regarding K_S values, the value of K_{AC} was similar to widely accepted numbers. In the case of K_{VFA} , several calibration attempts at different initial points showed that the solution was insensitive to its value. That is the reason why K_{VFA} was set to a default value (arbitrarily low (Puyol et al., 2017)) and $k_{M,vfa}$ was calibrated. In agreement with previous literature, these results show that acetate uptake is faster than for other VFAs, but also has a higher K_S .

Regarding biomass composition, the resulting values were similar to those from the literature. The small confidence intervals (particularly for N_{XB}) confirm the relevance of properly determining these values for an accurate prediction of the nutrient concentrations.

The corresponding parity plots (R^2 of 0.97-0.99; Figure S4) further confirm the validity of the model and parameters. Small confidence intervals also serve to identify the related processes as highly relevant.

3.2. Model validation

3.2.1. Application of the model to predict batch reactors: anaerobic vs. aerobic

To validate the calibrated ePAnM, data from batch reactors under both anaerobic and aerobic conditions were used. Figure 3 shows the corresponding experimental and modelling results.

Starting with the anaerobic conditions (Figures 3A, 3C, and 3E), the model was able to accurately represent the dynamics of both organic matter (as SCOD) and nutrients (for both N and P). This confirms that the calibrated parameters shown in Table 2 can be used to predict,

not only the dynamics in anaerobic batch PPB reactors, but also the nutrient composition of the resulting biomass. The slightly lower predicted final nutrient concentrations (particularly for N) might be related to the release of N from particulates present in the inoculum (not accounted for in the simulation). The TCOD concentrations were also accurately predicted, indicating that the model was able to reproduce biomass growth (Figure S5).

The calibrated model was also able to represent the faster uptake kinetics under aerobic conditions (Figures 3B, 3D, and 3F), and the lower biomass yields due to respiration (see Figure S5 for TCOD and DO concentrations). We note that the DO profiles were not a fit target. We simply wanted to provide enough oxygen to ensure aerobic conditions. If needed, k_{La} values could be dynamically calibrated to improve the DO predictions. The slightly higher differences between the modelled and the experimental data for nutrient consumption (particularly for P uptake) might be related to the change in growth mode, *i.e.*, aerobic *vs.* anaerobic, as different metabolisms might differ in nutrient uptake ratios. As the model was calibrated using data from an anaerobic reactor, this might lead to small errors under aerobic conditions. If needed, the parameters corresponding to the biomass composition grown under aerobic conditions could be recalibrated. This would result in more accurate predictions of the nutrient profiles under aerobic conditions.

The accurate prediction of the fast nutrient release after total SCOD consumption (around 0.5 d), indicates that the model was able to account for the relevance of predators under aerobic conditions (Figure 3). This agrees with previous results obtained aerating PPB enriched cultures (Capson-Tojo et al., 2021).

The model also predicted the predominant clades under the tested conditions, accounting for wash-out and out-competition. On the one hand, anaerobic-illuminated conditions resulted in growth of PPB, together with fermenters generating the VFAs that PPB consumed. On the other, aerobic conditions resulted in PPB outcompetition by aerobic heterotrophs due to the

faster growth rates of the later (Figure S6), and eventually lead to the development of aerobic grazers. These results agree with those obtained experimentally (Capson-Tojo et al., 2021).

Altogether, the results confirm that the proposed model can be applied to accurately represent the performance of PPB-enriched cultures under both aerobic and anaerobic conditions in batch reactors. This is highly relevant, not only to represent these systems separately, but also to account for competition between PPB and aerobic heterotrophs in open cultivations system, which might be exposed to oxygen via diffusion (*e.g.*, open ponds). These results further put the controversy around the option of non-sterile aerobic PPB cultivation to rest.

3.2.2. Model validation using pilot data

Long-term validation was done on a separate data set from the outdoors demonstration-scale PBR fed with poultry-processing wastewater. During the modelled period, the temperature ranged between 9.2 °C and 25 °C, and the peak light intensity between 325 W·m⁻² and 788 W·m⁻². The OLR also varied considerably, according to the COD concentration in the influent, ranging from 448 to 1,807 mg COD·L⁻¹·d⁻¹ (see Figure S7 for environmental conditions and substrate loads; see Appendix D.3 for the calculation of the daily light distributions).

Despite these wide variations in environmental conditions and influent characteristics, the model was able to represent the COD and nutrient concentrations in the PBR (Figure 4; see Figure S8 for X_C, X_I, and S_I concentrations in the reactor and the corresponding modelled results). The overall concentrations of SCOD and TCOD were accurately predicted. Despite their generally low values, the daily variations in S_{AC} and S_{VFA} concentrations were also predicted reasonably well (although the sampling frequency did not allow to assess daily fluctuations). The model was able to simulate the almost complete consumption of S_{AC} during most of the modelled period, caused by the availability of light at the time of sampling (10 am-12 pm). In addition, the S_{AC} and S_{VFA} increases during periods of low availability (*i.e.*,

early morning and late afternoon) were also represented accurately. It is important to consider that feeding only occurred during daytime. The few unmatching points showing slightly higher VFA concentrations can be explained by transient mixing issues in the reactor, which lead to temporary VFA peaks due to solids accumulation, which the model could not predict. Finally, the S_{IN} and S_{IP} profiles were accurately predicted, confirming the applicability of the calibrated biomass compositions under anaerobic conditions in flat plate PBRs (Table 2).

The accurate predictions of the COD and nutrient concentrations indicate that the model was also able to predict the reactor performance in terms of removal efficiencies and biomass productivities. The latter are shown in Figure S9. The obtained values (13-28 g COD·m⁻²·d⁻¹ considering only volatile solids) are in agreement with those commonly estimated from SCOD removal values (Hülßen et al., 2022b). These predicted productivities are difficult to determine experimentally if the wastewater has high solid contents, as additional measurements (*e.g.*, pigments contents) are required to differentiate between solids as biomass and solids remaining from the influent (Hülßen et al., 2020). Therefore, the model predictions can be used to estimate the actual biomass fraction in the harvested solids, which in turn can be used to estimate the biomass composition and thus its final value (*e.g.*, crude protein and ash contents when considering its application as SCP). The model can also predict overall productivities, including inert fractions. This is extremely useful, as it can be used to forecast if a waste stream will result in a profitable product or not (see Figure S10 for the modelled volatile/total solid ratio (VS/TS) and the biomass yields).

Other than the overall biomass productivities, the model also predicted the structure of the microbial communities (always considering that correlations between biomass decay and yield values exist). The modelled period (under anaerobic-illuminated conditions) resulted in predominant PPB growth, accompanied by fast-growing fermenters that generated VFAs from the complex organics entering the PBR (Figure S9). This symbiotic relationship, where

fermenters produce VFAs and PPB consume them, has been previously reported in processes treating wastewater using PPB enriched cultures (Hülßen et al., 2022b, 2022a, 2016b). Considering the microbial complexity of these systems, including bacterial clades other than PPB in the model is crucial to obtain an accurate prediction of the behaviour of these processes. This is not only useful to represent the process dynamics, but also to estimate the composition of the obtained biomass, and, most importantly, to troubleshoot and predict working/design parameters and situations where PPB might be outcompeted by other microorganisms. Further work should focus on the validation of these results using different reactor configurations (*e.g.*, open ponds).

3.3. Simulation of different scenarios

3.3.1. Predicting optimal operational conditions and reactor design in flat plate PBRs

The presented ePANM was used to estimate potential optimal operational and design parameters in PPB flat plate PBRs, namely the HRT and the reactor width (varied independently). The corresponding VFA removal efficiencies at steady state (used as performance criteria) are shown in Figure 5.

Starting with the HRT (Figure 5A), minimum values of 0.5 d must be kept if PPB biomass washout is to be avoided, thus keeping an efficient process performance. This implies that in semicontinuous outdoors flat plate reactors fed only during daytime, an overall HRT of 1 d must be kept, which agrees with previous limits presented in the literature (Hülßen et al., 2022b).

Figure 5B shows the VFA removal performance at different widths of a flat plate PBR at common averages daily light intensities ($150 \text{ W}\cdot\text{m}^{-2}$) and influent COD concentrations ($1,500 \text{ mg COD}\cdot\text{L}^{-1}$) (using the attenuation parameters from Capson-Tojo et al. (2022)). The performance fell drastically at widths over 10-20 cm, due to light attenuation through the reactor, mostly caused by light absorption by pigmented biomass (Capson-Tojo et al., 2022).

It must be considered that this dimension limit will vary according to many factors, such as the PPB biomass concentration, or the material used to build the reactor and the width of the walls themselves. These factors can potentially have a significant effect on light attenuation by the reactor walls (*e.g.*, via light reflection and refraction), and must therefore be considered. To allow for a comparison with open systems, and according to previous results using similar materials (Capson-Tojo et al., 2022), these simulations were carried out considering that no light was lost when passing through the reactor walls. In addition, it was assumed that light was equally received at both sides of the reactor, and that no solids other than biomass were present in the reactor. Therefore, these results represent an ideal situation for a flat plate system, and the provided dimension limit (reactor width of 10-20 cm) is likely to be more constrained in reality, especially when only illuminated from one side (or the reactor top).

Simulations at different OLRs (Figure S11A) suggest that, provided that the total HRT values are above 0.5 d, and that the pH is maintained within non-inhibitory ranges (achieved in the simulations via high N contents in the wastewater), the OLR limit will be given by the maximum biomass concentration allowing efficient light distribution in the reactor. Therefore, no substrate-induced inhibition due to excessive OLRs is expected when considering common COD concentrations in most wastewaters. Nevertheless, for proper nutrient recovery, the COD:N:P ratio in the wastewater is crucial to avoid reactor overloading and acidification. In this case, if the N and P contents are too low for a given COD concentration, the fermenters in the reactor will generate VFAs, which will not be consumed by PPB because nutrient deficiency will limit effective phototrophic growth. A sufficient N concentration is crucial, as it is not only needed for growth, but it also helps to keep the pH above acidifying values, as $\text{NH}_3\text{-N}$ is generated during fermentation. This effect can be observed in simulations carried out at different COD:N ratios (Figure S11B). Obviously, the alkalinity of the media and

potential buffering pairs present will also impact this phenomenon. It is interesting to consider that some of the electron disposal mechanisms of PPB occurring at low N contents (*e.g.*, nitrogenase-derived H₂ production or PHA accumulation) might alleviate the acidification effect at high COD:N ratios. Nevertheless, the slow kinetics of these processes compared to VFA generation by heterotrophic fermenters will reduce their potential impact on the pH via VFA consumption.

3.3.2. Simulating day-anaerobic/night-aerobic continuous operation

To predict the effects of continuous day and night feeding in 12 h intervals of anaerobic-illuminated and aerobic-dark conditions (recently proposed in the literature (Hülßen et al., 2022b)), simulations of this day-anaerobic/night-aerobic combined approach at different HRTs (1 and 2 d) were performed. The resulting concentrations of VFAs, nutrients (*e.g.*, N and P), and PPB biomass are shown in Figure 6. For comparison purposes, the corresponding results from fully aerated and fully anaerobic equivalent reactors are also presented.

Starting with the fully aerated reactor, the results at any tested HRTs show that, while this option can provide an effective removal of COD, the corresponding nutrient removal is much lower than in the other options (*i.e.*, intermittent aeration of fully anaerobic). This is a consequence of the predominant aerobic conditions, that result in PPB outcompetition by aerobic heterotrophs (see Figure 6; Figure S12 for concentrations of aerobes), with lower biomass yields. For the same reason (and due to growth of aerobic predators), biomass productivities were also significantly reduced in the fully aerated reactor (Figure S12). Basically, under full aeration the PBR is effectively transformed into an expensive high-rate activated sludge reactor.

The fully anaerobic system showed a typical behaviour in PPB-dominated reactors. During daytime, light enabled photoheterotrophic PPB growth, efficiently removing both COD and nutrients at biomass productivities over 15 g VS·m⁻²·d⁻¹ (*vs.* 6 g VS·m⁻²·d⁻¹ in the fully

aerated system, VS being volatile solids). Nevertheless, during night hours no effective growth occurred, which resulted in accumulation of organics and nutrients. At lower HRTs, this accumulation phenomenon was more pronounced, resulting in higher VFA and nutrient peaks. Because of this reduced treatment performance, lowering the HRT did not result in considerably higher productivities (Figure S12), with average values even slightly higher at an HRT of 2 d.

The combined day-anaerobic/night-aerobic process was able to exploit the benefits of both redox conditions. As in the fully aerated system, the combined process was able to maintain negligible VFA concentrations in the reactor at all times, meaning that night aeration was able to efficiently remove organics during the hours lacking sunlight. Regarding nutrients, the predominance of aerobic metabolism at night resulted in a lower average nutrient removal than in the fully anaerobic system. Nevertheless, this effect can be minimised by maintaining low HRTs (see Figure 6). This positive effect of low HRTs can be attributed to the washout of aerobic grazers/predators (they have lower growth rates compared to both PPB and aerobic heterotrophs), as well as to regular aerobic/anaerobic interval changes inhibiting the growth of predators during daytime. The predatory effect can also be observed when looking at the PPB concentrations, which are higher at an HRT of 1 d (Figure 6E). Therefore, low HRTs avoided the nutrient release caused by predation. Indeed, the average nutrient concentrations (and thus removal efficiencies) in the combined and the fully anaerobic reactors at 1 d HRT were almost equal. Interestingly, simulation results show that PPB were responsible, not only for treatment during daytime, but also during night hours. This indicates that PPB performed efficient heterotrophic growth during the night, which resulted in overall outcompetition of aerobic heterotrophs thanks to the higher concentrations of PPB biomass in the reactor (resulting from the anaerobic-illuminated periods). This can be confirmed by the high concentrations of PPB biomass in the reactor (Figure 6) and by the low concentrations or

aerobes (Figure S12). The average biomass productivities in the combined process (of around 12-13 g VS·m⁻²·d⁻¹) were also similar to those achieved in the fully anaerobic reactor at an HRT of 1.

Applying this combined aerobic/anaerobic process, Hülsen et al. (2022b) observed the emergence of aerobic bacteria (*e.g.*, *Brachymonas sp.*) in the PBR, which was likely caused by over aeration and long HRT. Here, we confirm the general applicability (theoretically) of this concept. Nevertheless, additional experiments, including the effects of aerobic/anaerobic intervals on the growth of common aerobic grazers, are needed to study and confirm the feasibility of the proposed day-anaerobic/night-aerobic continuous operation. The presented results show that this approach has a great potential to improve the performance of PPB outdoors PBRs, which would extend the wastewater treatment from semi-continuous to continuous day and night operation (highly relevant for various industries).

3.4. Implications for industrial application and further development

The presented model is the first mechanistic model that can be applied for simulation of PPB-enriched cultures grown outdoors, considering the main bacterial clades involved in these systems and varying environmental conditions. The obtained results show that, after calibration, the model was able to represent both batch and semicontinuous processes in batch (flasks) and flat plate reactors. Varying environmental conditions did not affect the prediction capabilities of the model.

The model can be directly applied to estimate the operational costs and the benefits of PPB outdoors reactors under the aforementioned configurations and different operational conditions. Recalibration and validation might be needed for other reactor types (*e.g.*, open ponds, bubble columns, or packed bed reactors). The model was able to predict the biomass productivities (including microbial communities and thus protein contents) and the effluent characteristics, which could be directly applied to estimate the revenues from the SCP-rich

product and the discharge costs savings. In addition, the model could also be applied to predict the amount of extra COD that could be necessary to further eliminate the N and P concentrations in the effluent (as in Puyol et al. (2017)), allowing to further detail the economic feasibility of this approach, even when using different COD sources.

The simulations show that PPB can withstand high substrate loads, provided that the illuminated HRT is maintained above 0.5-0.6 d⁻¹, avoiding PPB washout. The OLR by itself might not be a limitation, but the resulting high biomass concentrations at high loads will surely cause light availability issues, limiting the applicable OLR. In an analogous situation to that commonly occurring in anaerobic digesters, PPB reactors might be acidified, which will stop the process due to VFA accumulation and the consequent pH drop. High COD concentrations in the influent might result in VFA build-up when the COD:N ratios are too high, as VFA cannot be used for microbial growth. In terms of reactor design, model predictions show that reactor widths around 10 cm provide optimal treatment capabilities (for flat plate PBRs), which is in agreement with the literature on these reactors (Capson-Tojo et al., 2022).

PPB process can be operated at low HRTs and elevated OLRs (due to their relatively fast growth rates), which is a clear advantage when compared to other options for resource recovery. Compared to other phototrophic alternatives, such as microalgae, PBRs/ponds based on the latter are commonly operated at HRTs around 6 d, resulting in large reactor volumes, with high capital costs and/or large areal requirements (Robles et al., 2020a). Nevertheless, a potential drawback of PPB processes compared to microalgae is the lower light penetration in PPB reactors, which eventually results in smaller reactor widths or pond depths. However, this could be partly compensated by the generally lower light requirements of PPB. Microalgal ponds are commonly around 30 cm deep (Robles et al., 2020a), a value that should likely be reduced to 10-15 cm in PPB systems if an efficient VFA removal is to be

maintained. This might limit the performance of PPB ponds (also due to continuous oxygen diffusion), restricting their design possibilities and favouring more expensive PBRs. Further experimental research should be carried out to confirm optimal spacing. If the ePANM is to be used for ponds, dedicated validations (and probably recalibrations), should be performed.

The model also predicted that, while continuous aeration results in PPB outcompetition (in agreement with the literature (Capson-Tojo et al., 2021)), the combined day-anaerobic/night-aerobic continuous operation is a potential strategy to improve the performance of outdoors PPB reactors, particularly at low HRTs. Other approaches, such as a combined NIR/VIS illuminated reactors, where PPB grow photoheterotrophically and algae further polish the effluent, could also be tested. Experiments should be carried out to evaluate these options.

Further modelling developments should focus on predicting the product profile depending on influent characteristics and operational parameters, simulating the concentrations and production rates of other products (*e.g.*, hydrogen, PHA, or carotenoids). This could allow the prediction of the most suitable product (or combinations of) based on the influent characteristics, while optimising the working conditions to maximise the desired productivities. The development of a combined metabolic-mechanistic model (as in Santos et al. (2020)) would be an interesting approach for this purpose. The calibration of the model under different conditions/configurations would also allow to extend the model applicability and accuracy, validating its utilization in other reactor types. Similarly, estimation of kinetic parameters with different substrates and temperatures ranges, and particularly at extremely low and high light intensities, should also be performed. While a lumped parameter implementation (mixed tank) has been shown to be suitable for both flat plate and batch reactors here, this can be applied in a distributed parameter configuration to optimise light delivery, particularly relevant for non-incident light. Models developed during years of microalgae research could be translated to suit PPB reactors (Ación Fernández et al., 1997;

Béchet et al., 2013). Other modelling approaches previously applied for microalgae and not evaluated here, such as computational fluid dynamics (Ranganathan et al., 2022) or heat transfer modelling (Todisco et al., 2022) could also be adapted for PPB reactors, aiding in reactor design and process optimization.

4. Conclusions

The ePAnM accurately predicted the experimental data and showed the relevance of considering varying environmental conditions and other microbial clades. Results suggest that a minimum HRT of 0.5-0.6 d⁻¹ should be kept, and that high COD:N ratios can lead to acidification. The width of flat plate reactors should not exceed 10 cm. Simulations showed the potential of a day-anaerobic/night-aerobic approach in outdoor systems, which could enable efficient and continuous wastewater treatment, while maintaining high biomass productivities in a PPB dominated reactor. Future research and model development should be directed towards the prediction of product distribution in PPB.

Declaration of interests

The authors declare that they have no known competing financial interests or personal relationships that could have appeared to influence the work reported in this paper.

Acknowledgements

Gabriel Capson-Tojo acknowledges the Xunta de Galicia (postdoctoral fellowship ED481B-2018/017). Tim Hülsen is grateful to The Queensland Government, GHD, Ridley, Aquatec Maxcon and Ingham for financial support (Advanced Queensland Industry Fellowship).

References

- Acién Fernández, F.G., García Camacho, F., Sánchez Pérez, J.A., Fernández Sevilla, J.M., Molina Grima, E., 1997. A model for light distribution and average solar irradiance inside outdoor tubular photobioreactors for the microalgal mass culture. *Biotechnol. Bioeng.* 55, 701–714. [https://doi.org/10.1002/\(SICI\)1097-0290\(19970905\)55:5<701::AID-BIT1>3.0.CO;2-F](https://doi.org/10.1002/(SICI)1097-0290(19970905)55:5<701::AID-BIT1>3.0.CO;2-F)
- Akbari, L., Mahmoodzadeh Vaziri, B., 2017. Comprehensive modeling of photo-fermentation process for prediction of hydrogen production. *Int. J. Hydrogen Energy* 42, 14449–14457. <https://doi.org/10.1016/j.ijhydene.2017.04.119>
- Alloul, A., Cerruti, M., Adamczyk, D., Weissbrodt, D.G., Vlaeminck, S., 2021. Operational Strategies to Selectively Produce Purple Bacteria for Microbial Protein in Raceway Reactors. *Environ. Sci. Technol.* 55, 8278–8286. <https://doi.org/https://doi.org/10.1021/acs.est.0c08204>
- Batstone, D., 2021. Generalised Physicochemical Model No. 1 (PCM1) for Water and Wastewater Treatment. IWA Publishing.
- Batstone, D.J., Hülsen, T., Mehta, C.M., Keller, J., 2015. Platforms for energy and nutrient recovery from domestic wastewater: A review. *Chemosphere* 140, 2–11. <https://doi.org/10.1016/j.chemosphere.2014.10.021>
- Batstone, D.J., Hülsen, T., Oehmen, A., 2019. Metabolic modelling of mixed culture anaerobic microbial processes. *Curr. Opin. Biotechnol.* 57, 137–144. <https://doi.org/10.1016/j.copbio.2019.03.014>
- Batstone, D.J., Keller, J., Angelidaki, I., Kalyuzhny, S. V., Pavlostathis, S.G., Rozzi, A., Sanders, W.T.M., Siegrist, H., Vavilin, V.A., 2002. Anaerobic digestion model no. 1 (ADM1). IWA Publishing. <https://doi.org/https://doi.org/10.2166/wst.2002.0292>
- Béchet, Q., Shilton, A., Guieysse, B., 2013. Modeling the effects of light and temperature on algae growth: State of the art and critical assessment for productivity prediction during outdoor cultivation. *Biotechnol. Adv.* 31, 1648–1663. <https://doi.org/10.1016/j.biotechadv.2013.08.014>
- Bernard, O., Rémond, B., 2012. Validation of a simple model accounting for light and temperature effect on microalgal growth. *Bioresour. Technol.* 123, 520–527. <https://doi.org/10.1016/j.biortech.2012.07.022>
- Capson-Tojo, G., Batstone, D.J., Grassino, M., Hülsen, T., 2022. Light attenuation in enriched purple phototrophic bacteria cultures: implications for modelling and reactor design. *Water Res.* 219, 118572. <https://doi.org/doi.org/10.1016/j.watres.2022.118572>
- Capson-Tojo, G., Batstone, D.J., Grassino, M., Vlaeminck, S.E., Puyol, D., Verstraete, W., Kleerebezem, R., Oehmen, A., Ghimire, A., Pikaar, I., Lema, J.M., Hülsen, T., 2020a. Purple phototrophic bacteria for resource recovery: Challenges and opportunities. *Biotechnol. Adv.* 43, 107567. <https://doi.org/doi.org/10.1016/j.biotechadv.2020.107567>
- Capson-Tojo, G., Lin, S., Batstone, D.J., Hülsen, T., 2021. Purple phototrophic bacteria are outcompeted by aerobic heterotrophs in the presence of oxygen. *Water Res.* 194, 116941. <https://doi.org/10.1016/j.watres.2021.116941>
- Capson-Tojo, G., Moscoviz, R., Astals, S., Robles, A., Steyer, J.-P., 2020b. Unraveling the literature chaos around free ammonia inhibition in anaerobic digestion. *Renew. Sustain. Energy Rev.* 117, 109487. <https://doi.org/10.1016/j.rser.2019.109487>
- Casagli, F., Zuccaro, G., Bernard, O., Steyer, J.P., Ficara, E., 2021. ALBA: A comprehensive growth model to optimize algae-bacteria wastewater treatment in raceway ponds. *Water*

- Res. 190, 116734. <https://doi.org/10.1016/j.watres.2020.116734>
- Dalaei, P., Ho, D., Nakhla, G., Santoro, D., 2019. Low temperature nutrient removal from municipal wastewater by purple phototrophic bacteria (PPB). *Bioresour. Technol.* 288, 121566. <https://doi.org/10.1016/j.biortech.2019.121566>
- Darvehei, P., Bahri, P.A., Moheimani, N.R., 2018. Model development for the growth of microalgae: A review. *Renew. Sustain. Energy Rev.* 97, 233–258. <https://doi.org/10.1016/j.rser.2018.08.027>
- Day, J.G., Gong, Y., Hu, Q., 2017. Microzooplanktonic grazers – A potentially devastating threat to the commercial success of microalgal mass culture. *Algal Res.* 27, 356–365.
- Durán, F., Robles, Á., Giménez, J.B., Ferrer, J., Ribes, J., Serralta, J., 2020. Modelling the anaerobic treatment of sulfate-rich urban wastewater: application to AnMBR technology. *Water Res.* 184, 116133.
- Egger, F., Hülsen, T., Tait, S., Batstone, D.J., 2020. Autotrophic sulfide removal by mixed culture purple phototrophic bacteria. *Water Res.* 182, 115896. <https://doi.org/10.1016/j.watres.2020.115896>
- Gadhamshetty, V., Sukumaran, A., Nirmalakhandan, N., Thein Myint, M., 2008. Photofermentation of malate for biohydrogen production- A modeling approach. *Int. J. Hydrogen Energy* 33, 2138–2146. <https://doi.org/10.1016/j.ijhydene.2008.02.046>
- Hädicke, O., Grammel, H., Klamt, S., 2011. Metabolic network modeling of redox balancing and biohydrogen production in purple nonsulfur bacteria. *BMC Syst. Biol.* 5, 150. <https://doi.org/10.1186/1752-0509-5-150>
- Henze, M., Gujer, W., Mino, T., van Loosdrecht, M.C.M., 2000. Activated Sludge Models ASM1, ASM2, ASM2d and ASM3. IWA Publishing.
- Henze, M., Harremoës, P., la Cour Jansen, J., Arvin, E., 2002. Wastewater Treatment, Biological and chemical processes, 3rd ed. Springer.
- Hülsen, T., Barry, E.M., Lu, Y., Puyol, D., Batstone, D.J., 2016a. Low temperature treatment of domestic wastewater by purple phototrophic bacteria: Performance, activity, and community. *Water Res.* 100, 537–545. <https://doi.org/10.1016/j.watres.2016.05.054>
- Hülsen, T., Barry, E.M., Lu, Y., Puyol, D., Keller, J., Batstone, D.J., 2016b. Domestic wastewater treatment with purple phototrophic bacteria using a novel continuous photo anaerobic membrane bioreactor. *Water Res.* 100, 486–495. <https://doi.org/10.1016/j.watres.2016.04.061>
- Hülsen, T., Batstone, D.J., Keller, J., 2014. Phototrophic bacteria for nutrient recovery from domestic wastewater. *Water Res.* 50, 18–26. <https://doi.org/10.1016/j.watres.2013.10.051>
- Hülsen, T., Hsieh, K., Batstone, D.J., 2019. Saline wastewater treatment with purple phototrophic bacteria. *Water Res.* 160, 259–267. <https://doi.org/10.1016/j.watres.2019.05.060>
- Hülsen, T., Hsieh, K., Lu, Y., Tait, S., Batstone, D.J., 2018. Simultaneous treatment and single cell protein production from agri-industrial wastewaters using purple phototrophic bacteria or microalgae – A comparison. *Bioresour. Technol.* 254, 214–223. <https://doi.org/10.1016/j.biortech.2018.01.032>
- Hülsen, T., Sander, E.M., Jensen, P.D., Batstone, D.J., 2020. Application of purple phototrophic bacteria in a biofilm photobioreactor for single cell protein production: Biofilm vs suspended growth. *Water Res.* 181, 115909. <https://doi.org/10.1016/j.watres.2020.115909>
- Hülsen, T., Stegman, S., Batstone, D.J., Capson-Tojo, G., 2022a. Naturally illuminated photobioreactors for resource recovery from piggery and chicken-processing wastewaters utilising purple phototrophic bacteria. *Water Res.* 214, 118194.

- <https://doi.org/doi.org/10.1016/j.watres.2022.118194>
- Hülßen, T., Züger, C., Batstone, D.J., Solley, D., Ochre, P., Porter, B., Capson-Tojo, G., 2022b. Outdoor demonstration-scale flat plate photobioreactor for resource recovery with purple phototrophic bacteria. *Water Res.* 216, 118327. <https://doi.org/https://doi.org/10.1016/j.watres.2022.118327>
- Izu, K., Nakajima, F., Yamamoto, K., Kurisu, F., 2001. Aeration conditions affecting growth of purple nonsulfur bacteria in an organic wastewater treatment process. *Syst. Appl. Microbiol.* 24, 294–302. <https://doi.org/10.1078/0723-2020-00027>
- Jeppsson, U., Rosen, C., Alex, J., Copp, J., Gernaey, K. V., Pons, M.N., Vanrolleghem, P. a., 2006. Towards a benchmark simulation model for plant-wide control strategy performance evaluation of WWTPs. *Water Sci. Technol.* 53, 287–295. <https://doi.org/10.2166/wst.2006.031>
- Kim, M.K., Choi, K.M., Yin, C.R., Lee, K.Y., Im, W.T., Ju, H.L., Lee, S.T., 2004. Odorous swine wastewater treatment by purple non-sulfur bacteria, *Rhodospseudomonas palustris*, isolated from eutrophicated ponds. *Biotechnol. Lett.* 26, 819–822. <https://doi.org/10.1023/B:BILE.0000025884.50198.67>
- Klamt, S., Grammel, H., Straube, R., Ghosh, R., Gilles, E.D., 2008. Modeling the electron transport chain of purple non-sulfur bacteria. *Mol. Syst. Biol.* 4, 1–19. <https://doi.org/10.1038/msb4100191>
- Lu, H., Zhang, G., Zheng, Z., Meng, F., Du, T., He, S., 2019. Bio-conversion of photosynthetic bacteria from non-toxic wastewater to realize wastewater treatment and bioresource recovery: A review. *Bioresour. Technol.* 278, 383–399. <https://doi.org/10.1016/j.biortech.2019.01.070>
- Madigan, M.T., Martinko, J.M., Stahl, D.A., Clark, D.P., 2011. Metabolic Diversity and Commercial Biocatalyses, in: *Brock Biology of Microorganisms*. Pearson, pp. 346–350. <https://doi.org/10.1038/hr.2014.17>
- Moussa, M.S., Hooijmans, C.M., Lubberding, H.J., Gijzen, H.J., Van Loosdrecht, M.C.M., 2005. Modelling nitrification, heterotrophic growth and predation in activated sludge. *Water Res.* 39, 5080–5098. <https://doi.org/10.1016/j.watres.2005.09.038>
- Muñoz, R., Guieysse, B., 2006. Algal-bacterial processes for the treatment of hazardous contaminants: A review. *Water Res.* 40, 2799–2815. <https://doi.org/10.1016/j.watres.2006.06.011>
- Ni, B.-J., Sheng, G., Yu, H.-Q., 2011. Model-based characterization of endogenous maintenance, cell death and predation processes of activated sludge in sequencing batch reactors. *Chem. Eng. Sci.* 66, 747–754. <https://doi.org/10.1016/j.ces.2010.11.033>
- Obeid, J., Magnin, J.P., Flaus, J.M., Adrot, O., Willison, J.C., Zlatev, R., 2009. Modelling of hydrogen production in batch cultures of the photosynthetic bacterium *Rhodobacter capsulatus*. *Int. J. Hydrogen Energy* 34, 180–185. <https://doi.org/10.1016/j.ijhydene.2008.09.081>
- Posten, C., Schaub, G., 2009. Microalgae and terrestrial biomass as source for fuels-A process view. *J. Biotechnol.* 142, 64–69. <https://doi.org/10.1016/j.jbiotec.2009.03.015>
- Puyol, D., Barry, E.M., Hülßen, T., Batstone, D.J., 2017. A mechanistic model for anaerobic phototrophs in domestic wastewater applications: Photo-anaerobic model (PAnM). *Water Res.* 116, 241–253. <https://doi.org/10.1016/j.watres.2017.03.022>
- Puyol, D., Hülßen, T., Padrino, B., Batstone, D.J., Martinez, F., Melero, J.A., 2020. Exploring the inhibition boundaries of mixed cultures of purple phototrophic bacteria for wastewater treatment in anaerobic conditions. *Water Res.* 183, 116057. <https://doi.org/10.1016/j.watres.2020.116057>
- Ranganathan, P., Pandey, A.K., Sirohi, R., Tuan Hoang, A., Kim, S.H., 2022. Recent

- advances in computational fluid dynamics (CFD) modelling of photobioreactors: Design and applications. *Bioresour. Technol.* 350, 126920. <https://doi.org/10.1016/j.biortech.2022.126920>
- Robles, Á., Capson-Tojo, G., Gales, A., Ruano, M.V., Sialve, B., Ferrer, J., Steyer, J., 2020a. Microalgae-bacteria consortia in high-rate ponds for treating urban wastewater: Elucidating the key state indicators under dynamic conditions. *J. Environ. Manage.* 261, 110244. <https://doi.org/10.1016/j.jenvman.2020.110244>
- Robles, Á., Capson-Tojo, G., Gales, A., Viruela, A., Sialve, B., Seco, A., Steyer, J.-P., Ferrer, J., 2020b. Performance of a membrane-coupled high-rate algal pond for urban wastewater treatment at demonstration scale. *Bioresour. Technol.* 301, 122672. <https://doi.org/10.1016/j.biortech.2019.122672>
- Ruiz-Martínez, A., Serralta, J., Seco, A., Ferrer, J., 2016. Modeling light and temperature influence on ammonium removal by *Scenedesmus* sp. under outdoor conditions. *Water Sci. Technol.* 74, 1964–1970. <https://doi.org/10.2166/wst.2016.383>
- Santos, J.M.M., Rieger, L., Lanham, A.B., Carvalheira, M., Reis, M., Oehmen, A., 2020. A novel metabolic-ASM model for full-scale biological nutrient removal systems. *Water Res.* 115373. <https://doi.org/10.1016/j.watres.2019.115373>
- Shoener, B.D., Schramm, S.M., Béline, F., Bernard, O., Martínez, C., Plósz, B.G., Snowling, S., Steyer, J.P., Valverde-Pérez, B., Wágner, D., Guest, J.S., 2019. Microalgae and cyanobacteria modeling in water resource recovery facilities: A critical review. *Water Res.* X 2. <https://doi.org/10.1016/j.wroa.2018.100024>
- Solimeno, A., García, J., 2017. Microalgae-bacteria models evolution: From microalgae steady-state to integrated microalgae-bacteria wastewater treatment models – A comparative review. *Sci. Total Environ.* 607–608, 1136–1150. <https://doi.org/10.1016/j.scitotenv.2017.07.114>
- Solimeno, A., Gómez-Serrano, C., Ación, F.G., 2019. BIO_ALGAE 2: improved model of microalgae and bacteria consortia for wastewater treatment. *Environ. Sci. Pollut. Res.* 26, 25855–25868. <https://doi.org/10.1007/s11356-019-05824-5>
- Todisco, E., Louveau, J., Thobie, C., Dechandol, E., Hervé, L., Durécu, S., Titica, M., Pruvost, J., 2022. A dynamic model for temperature prediction in a façade-integrated photobioreactor. *Chem. Eng. Res. Des.* 181, 371–383. <https://doi.org/10.1016/j.cherd.2022.03.017>
- Wágner, D.S., Valverde-Pérez, B., Sæbø, M., Bregua de la Sotilla, M., Van Wagenen, J., Smets, B.F., Plósz, B.G., 2016. Towards a consensus-based biokinetic model for green microalgae – The ASM-A. *Water Res.* 103, 485–499. <https://doi.org/10.1016/j.watres.2016.07.026>
- Yetis, M., Gündüz, U., Eroglu, I., Yücel, M., Türker, L., 2000. Photoproduction of hydrogen from sugar refinery wastewater by *Rhodobacter sphaeroides* O.U. 001. *Int. J. Hydrogen Energy* 25, 1035–1041. [https://doi.org/10.1016/S0360-3199\(00\)00027-6](https://doi.org/10.1016/S0360-3199(00)00027-6)
- Zeilstra-Ryalls, J., Gomelsky, M., Eraso, J.M., Yeliseev, A., O’Gara, J., Kaplan, S., 1998. Control of photosystem formation in *Rhodobacter sphaeroides*. *J. Bacteriol.* 180, 2801–2809. <https://doi.org/10.1128/jb.180.11.2801-2809.1998>
- Zhang, D., Xiao, N., Mahbubani, K.T., del Rio-Chanona, E.A., Slater, N.K.H., Vassiliadis, V.S., 2015. Bioprocess modelling of biohydrogen production by *Rhodospseudomonas palustris*: Model development and effects of operating conditions on hydrogen yield and glycerol conversion efficiency. *Chem. Eng. Sci.* 130, 68–78. <https://doi.org/10.1016/j.ces.2015.02.045>

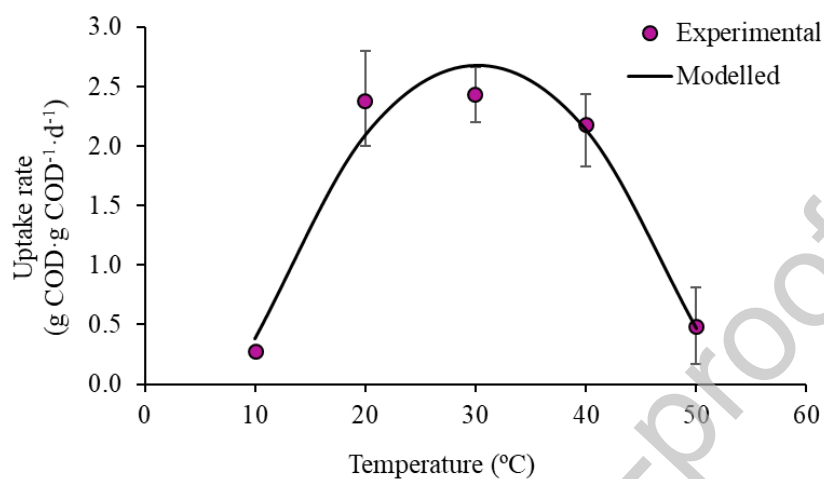


Figure 1. Maximum phototrophic specific uptake rates at different temperatures for enriched purple phototrophic bacteria cultures, and corresponding cardinal temperature model with inflexion curve. The error bars represent 95% confidence intervals.

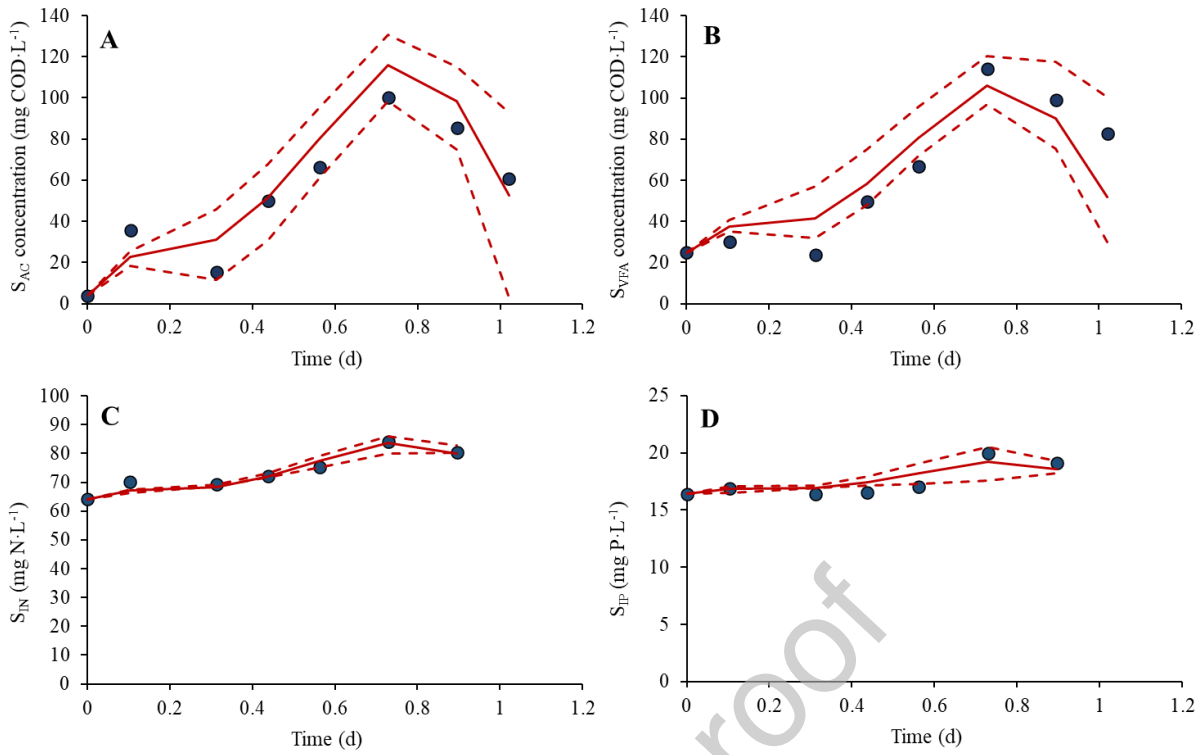


Figure 2. Experimental values from the cycle study used for model calibration and modelling results (including 95% prediction confidences) for (A) acetate (S_{AC}), (B) other volatile fatty acids (S_{VFA}), (C) inorganic nitrogen (S_{IN}), and (D) inorganic phosphorus (S_{IP}).

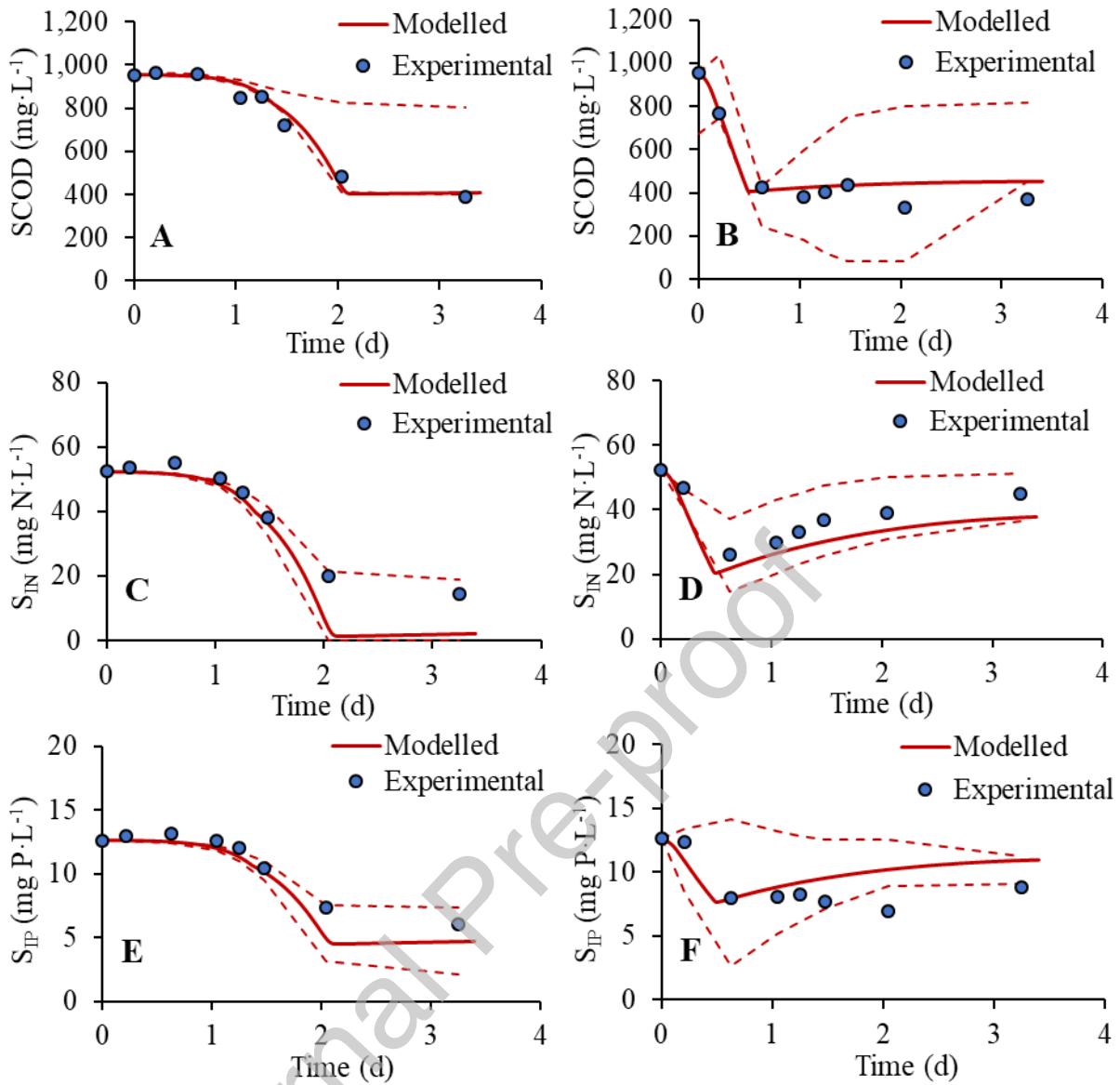


Figure 3. Experimental and modelled concentrations of soluble COD (SCOD), inorganic N (S_{IN}), and inorganic P (S_{IP}) from the batch reactors used for model validation: (A, C, E) anaerobic and (B, D, F) aerobic conditions. Dashed lines indicate 95% confidence intervals.

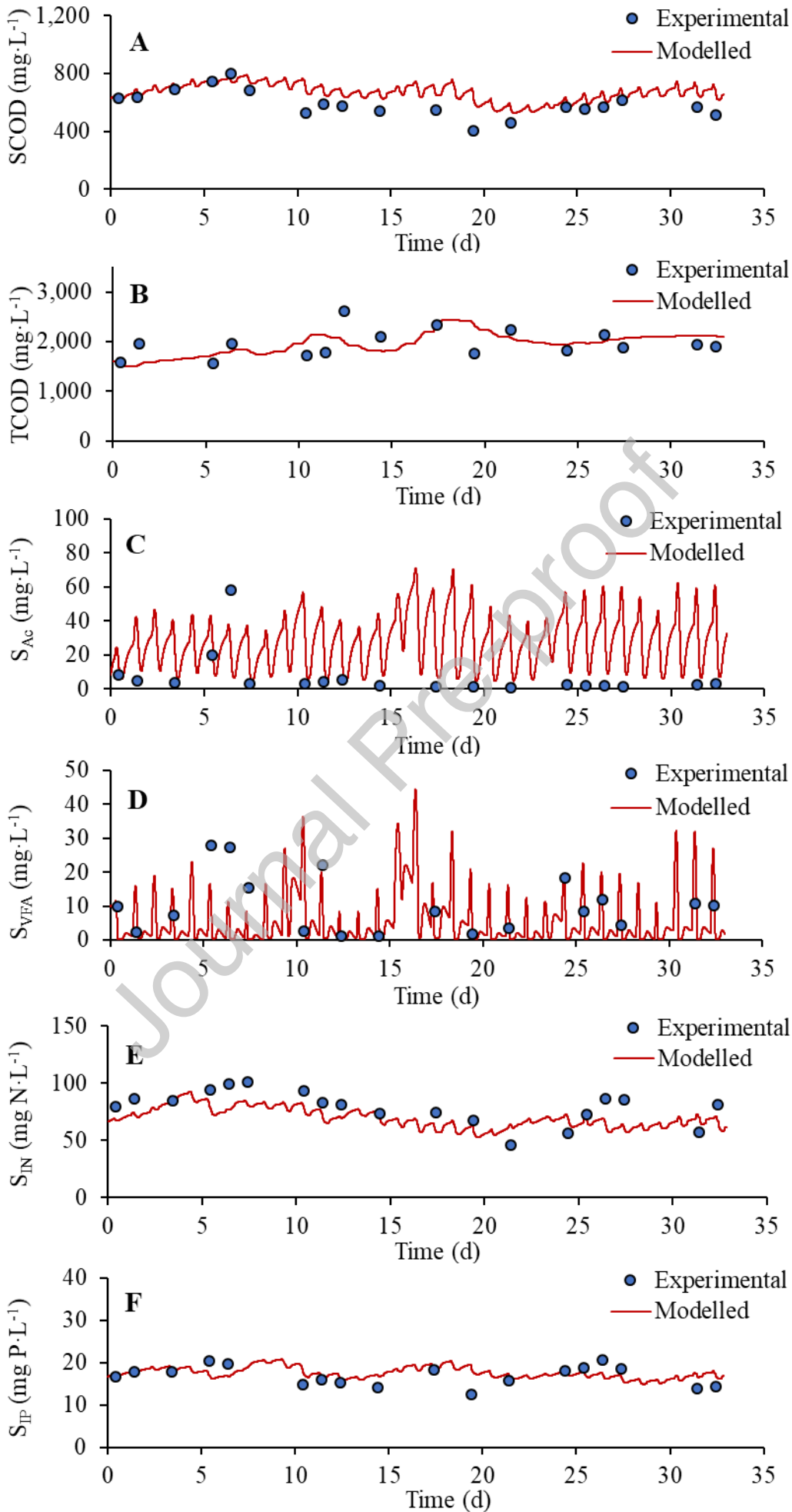


Figure 4. Experimental values and modelling results for the period from the demonstration flat plate reactor used for model validation. The concentrations of (A) soluble COD (SCOD), (B) total COD (TCOD), (C) acetate (S_{AC}), (D) other volatile fatty acids (S_{VFA}), (E) inorganic N (S_{IN}), and (F) inorganic P (S_{IP}) are shown.

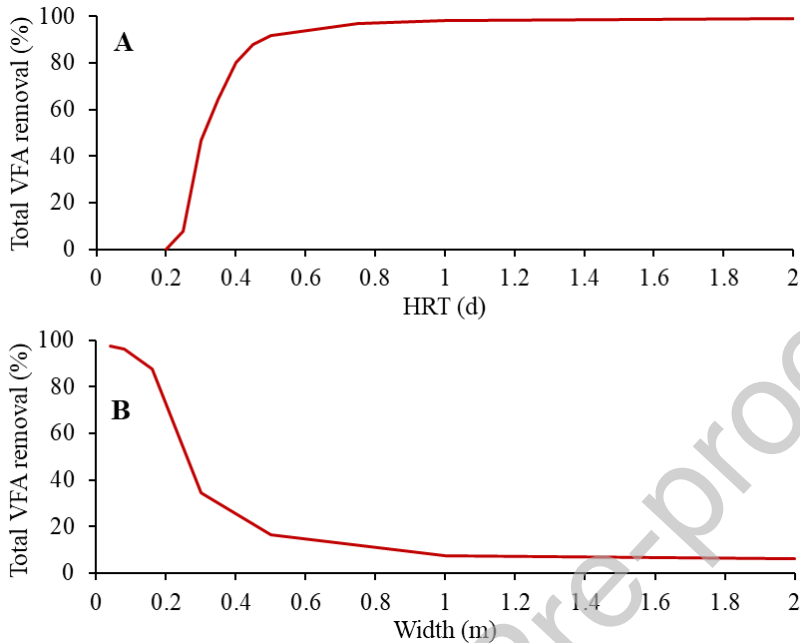


Figure 5. Simulation results showing the total volatile fatty acid (VFA) removal efficiencies in a flat plate reactor at different (A) hydraulic retention times (HRTs), and (B) reactor widths. Anaerobic, continuously illuminated conditions were assumed, with a filtered near infra-red fraction of 100%. Continuous feeding was provided, with an influent total VFAs concentration of 600-1,500 mg COD·L⁻¹. The simulation time was 30 d.

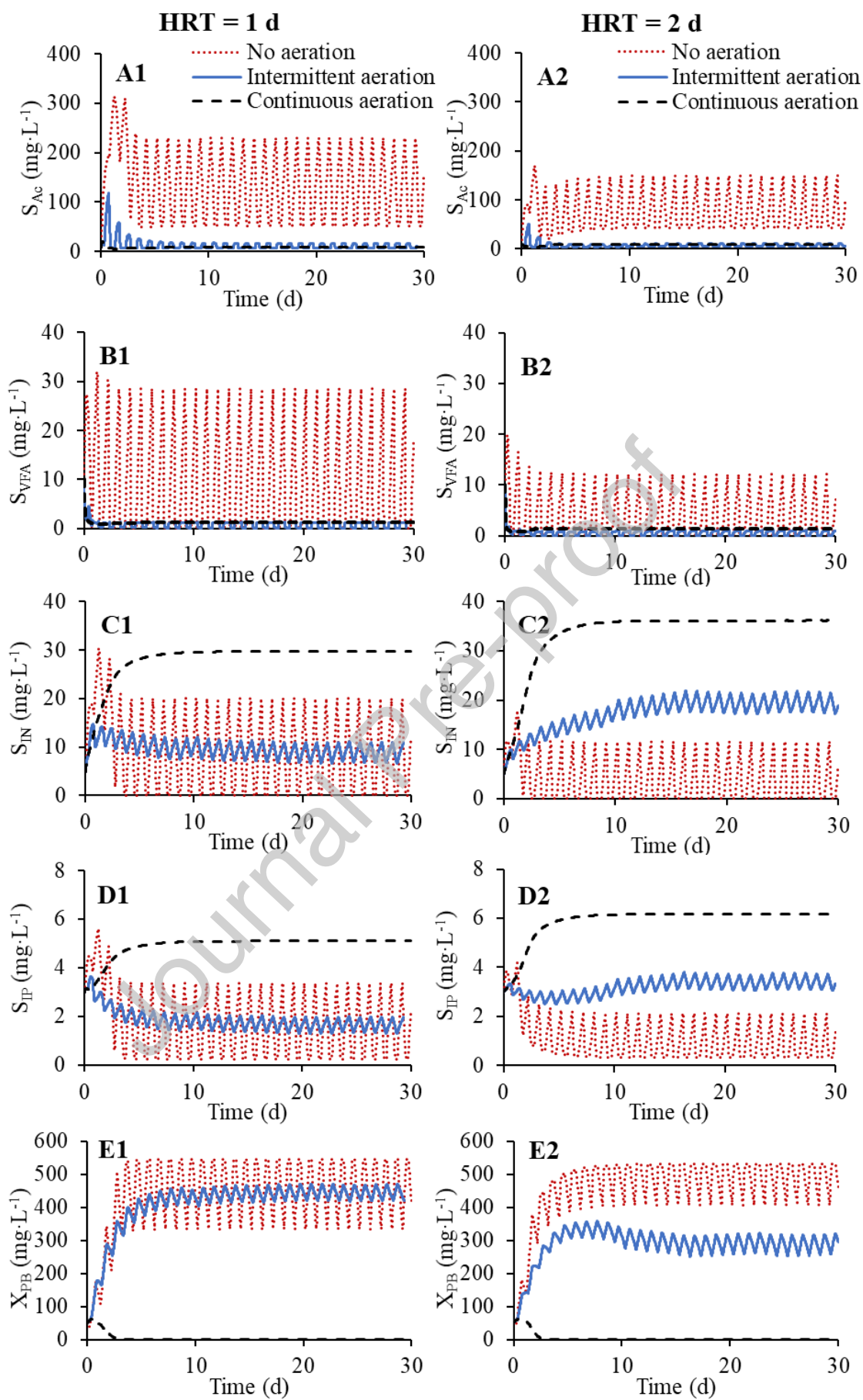


Figure 6. Simulation results showing the concentrations of (A) acetate (S_{AC}), (B) other volatile fatty acids (S_{VFA}), (C) inorganic nitrogen (S_{IN}), (D) inorganic phosphorus (S_{IP}), and (E) purple phototrophic bacteria biomass (X_{PB}) in an outdoors flat plate reactor working at a hydraulic retention time of (A1-E1) 1 d, and of (A2-E2) 2 d. Three aeration strategies are compared: no aeration, intermittent aeration during night-time, and continuous aeration. The reactor was continuously fed with an influent containing $600 \text{ mg COD}\cdot\text{L}^{-1}$ of volatile fatty acids. A natural illumination profile was assumed, with an incident near infra-red fraction in the reactor of 100%.

Journal Pre-proof

Table 1. Petersen matrix of the ePAnM. S represents soluble compounds, X particulates and the subscripts i and j denote compound and process.

Component	i	1	2	3	4	5	6	7	8	9	10	11	Rate (g COD m ⁻³ d ⁻¹)
1 Hydrolysis		S _{VFA}	S _{AC}	S _{IC}	S _{II}	S _O	S _{IN}	S _{IP}	S _{ORG,S}	S _I	S _{SO4}	S _S	$k_{HYD} \cdot X_{H1}$
2 Phototrophic acetate uptake by PPB			-1	f _{IC,VA,40}			$-\Sigma_{i=1,5,21} N_i \cdot V_{i,2}$	$-\Sigma_{i=1,6,21} P_i \cdot V_{i,2}$					$k_{M,VA} \frac{S_{VA}}{K_{M,VA} + S_{VA}} \cdot X_{PPB} \cdot I_{AN} \cdot I_{AC} \cdot I_{P} \cdot I_{I} \cdot I_{O} \cdot I_{SO4} \cdot I_T$
3 Phototrophic VFA uptake by PPB		-1		f _{IC,VA,48}			$-\Sigma_{i=1,5,21} N_i \cdot V_{i,3}$	$-\Sigma_{i=1,6,21} P_i \cdot V_{i,3}$					$k_{M,VFA} \frac{S_{VFA}}{K_{M,VFA} + S_{VFA}} \cdot X_{PPB} \cdot I_{AN} \cdot I_{AC} \cdot I_{P} \cdot I_{I} \cdot I_{O} \cdot I_{SO4} \cdot I_T$
4 VFA fermentation by PPB			(1-Y _{PPB,4})	f _{IC,VA,48}	(1-Y _{PPB,4})		$-\Sigma_{i=1,5,21} N_i \cdot V_{i,4}$	$-\Sigma_{i=1,6,21} P_i \cdot V_{i,4}$					$k_{M,FB} \frac{S_{VFA}}{K_{M,FB} + S_{VFA}} \cdot X_{PPB} \cdot I_{AN} \cdot I_{AC} \cdot I_{P} \cdot I_{I} \cdot I_{O} \cdot I_{SO4} \cdot I_T$
5 Organics fermentation by PPB	(1-Y _{PPB,5})		(1-Y _{PPB,5})	f _{IC,ORG}	(1-Y _{PPB,5})		$-\Sigma_{i=1,5,21} N_i \cdot V_{i,5}$	$-\Sigma_{i=1,6,21} P_i \cdot V_{i,5}$	-1				$k_{M,ORG} \frac{S_{ORG}}{K_{M,ORG} + S_{ORG}} \cdot X_{PPB} \cdot I_{AN} \cdot I_{AC} \cdot I_{P} \cdot I_{I} \cdot I_{O} \cdot I_{SO4} \cdot I_T$
6 Acetate uptake aerobically by PPB			-1	$-\Sigma_{i=1,2,4,21} C_{i,V,6}$		(-1-Y _{PPB,6})	$-\Sigma_{i=1,5,21} N_i \cdot V_{i,6}$	$-\Sigma_{i=1,6,21} P_i \cdot V_{i,6}$					$k_{M,O,PPB} \frac{S_{AC}}{K_{M,O,PPB} + S_{AC}} \cdot \frac{S_O}{K_{O,PPB} + S_O} \cdot X_{PPB} \cdot I_{AN} \cdot I_{AC} \cdot I_{P} \cdot I_{I} \cdot I_{O} \cdot I_{SO4} \cdot I_T$
7 VFA uptake aerobically by PPB		-1		$-\Sigma_{i=1,2,4,21} C_{i,V,7}$		(-1-Y _{PPB,7})	$-\Sigma_{i=1,5,21} N_i \cdot V_{i,7}$	$-\Sigma_{i=1,6,21} P_i \cdot V_{i,7}$					$k_{M,O,VFA} \frac{S_{VFA}}{K_{M,O,VFA} + S_{VFA}} \cdot \frac{S_O}{K_{O,PPB} + S_O} \cdot X_{PPB} \cdot I_{AN} \cdot I_{AC} \cdot I_{P} \cdot I_{I} \cdot I_{O} \cdot I_{SO4} \cdot I_T$
8 Organics uptake aerobically by PPB			-1	$-\Sigma_{i=1,2,4,21} C_{i,V,8}$		(-1-Y _{PPB,8})	$-\Sigma_{i=1,5,21} N_i \cdot V_{i,8}$	$-\Sigma_{i=1,6,21} P_i \cdot V_{i,8}$	-1				$k_{M,O,ORG} \frac{S_{ORG}}{K_{M,O,ORG} + S_{ORG}} \cdot \frac{S_O}{K_{O,PPB} + S_O} \cdot X_{PPB} \cdot I_{AN} \cdot I_{AC} \cdot I_{P} \cdot I_{I} \cdot I_{O} \cdot I_{SO4} \cdot I_T$
9 Acetate uptake by aerobes				$-\Sigma_{i=1,2,4,21} C_{i,V,9}$		(-1-Y _{Aer,9})	$-\Sigma_{i=1,5,21} N_i \cdot V_{i,9}$	$-\Sigma_{i=1,6,21} P_i \cdot V_{i,9}$					$k_{M,O,A} \frac{S_{AC}}{K_{M,O,A} + S_{AC}} \cdot \frac{S_O}{K_{O,A} + S_O} \cdot X_{Aer} \cdot I_{AN} \cdot I_{P} \cdot I_T$
10 VFA uptake by aerobes		-1		$-\Sigma_{i=1,2,4,21} C_{i,V,10}$		(-1-Y _{Aer,10})	$-\Sigma_{i=1,5,21} N_i \cdot V_{i,10}$	$-\Sigma_{i=1,6,21} P_i \cdot V_{i,10}$					$k_{M,O,A} \frac{S_{VFA}}{K_{M,O,A} + S_{VFA}} \cdot \frac{S_O}{K_{O,A} + S_O} \cdot X_{Aer} \cdot I_{AN} \cdot I_{P} \cdot I_T$
11 Organics uptake by aerobes				$-\Sigma_{i=1,2,4,21} C_{i,V,11}$		(-1-Y _{Aer,11})	$-\Sigma_{i=1,5,21} N_i \cdot V_{i,11}$	$-\Sigma_{i=1,6,21} P_i \cdot V_{i,11}$	-1				$k_{M,O,A} \frac{S_{ORG}}{K_{M,O,A} + S_{ORG}} \cdot \frac{S_O}{K_{O,A} + S_O} \cdot X_{Aer} \cdot I_{AN} \cdot I_{P} \cdot I_T$
12 Organics uptake by acidogens	(1-Y _{A1})		(1-Y _{A1})	$-\Sigma_{i=1,2,4,21} C_{i,V,12}$	(1-Y _{A1})		$-\Sigma_{i=1,5,21} N_i \cdot V_{i,12}$	$-\Sigma_{i=1,6,21} P_i \cdot V_{i,12}$					$k_{M,H} \frac{S_{ORG}}{K_{M,H} + S_{ORG}} \cdot X_{A1} \cdot I_{AN} \cdot I_{P} \cdot I_T$
13 VFA uptake by acetogens	(1-Y _{A2})		(1-Y _{A2})	$-\Sigma_{i=1,2,4,21} C_{i,V,13}$	(1-Y _{A2})		$-\Sigma_{i=1,5,21} N_i \cdot V_{i,13}$	$-\Sigma_{i=1,6,21} P_i \cdot V_{i,13}$					$k_{M,A} \frac{S_{VFA}}{K_{M,A} + S_{VFA}} \cdot X_{A2} \cdot I_{AN} \cdot I_{P} \cdot I_T$
14 Autotrophic uptake of H ₂ by PPB NIR				-f _{IC,H2}	-f _{II,H2}		$-\Sigma_{i=1,5,21} N_i \cdot V_{i,14}$	$-\Sigma_{i=1,6,21} P_i \cdot V_{i,14}$					$k_{M,C} \frac{S_{H2}}{K_{M,C} + S_{H2}} \cdot \frac{S_{CO2}}{K_{CO2} + S_{CO2}} \cdot X_{PPB} \cdot I_{AN} \cdot I_{AC} \cdot I_{P} \cdot I_{I} \cdot I_{O} \cdot I_{SO4} \cdot I_T$
15 Predation of aerobes by aerobic grazers				$-\Sigma_{i=1,2,4,21} C_{i,V,15}$		(-1-Y _{PPB,15})	$-\Sigma_{i=1,5,21} N_i \cdot V_{i,15}$	$-\Sigma_{i=1,6,21} P_i \cdot V_{i,15}$					$k_{M,PPB} \frac{X_{Aer}}{K_{M,PPB} + X_{Aer}} \cdot \frac{S_O}{K_{O,PPB} + S_O} \cdot X_{PPB} \cdot I_{AN} \cdot I_{P} \cdot I_T$
16 Predation of PPB by aerobic grazers				$-\Sigma_{i=1,2,4,21} C_{i,V,16}$		(-1-Y _{PPB,16})	$-\Sigma_{i=1,5,21} N_i \cdot V_{i,16}$	$-\Sigma_{i=1,6,21} P_i \cdot V_{i,16}$					$k_{M,PPB} \frac{X_{PPB}}{K_{M,PPB} + X_{PPB}} \cdot \frac{S_O}{K_{O,PPB} + S_O} \cdot X_{Aer} \cdot I_{AN} \cdot I_{P} \cdot I_T$
17 Acetate uptake by HSRB			-1	$-\Sigma_{i=1,2,4,21} C_{i,V,17}$			$-\Sigma_{i=1,5,21} N_i \cdot V_{i,17}$	$-\Sigma_{i=1,6,21} P_i \cdot V_{i,17}$			(-1-Y _{HSRB,17})	(-1-Y _{HSRB,17})	$k_{M,HSRB} \frac{S_{AC}}{K_{M,HSRB} + S_{AC}} \cdot \frac{S_{SO4}}{K_{S,HSRB} + S_{SO4}} \cdot X_{HSRB} \cdot I_{AN} \cdot I_{P} \cdot I_{SO4} \cdot I_T$
18 VFA uptake by HSRB		-1		$-\Sigma_{i=1,2,4,21} C_{i,V,18}$			$-\Sigma_{i=1,5,21} N_i \cdot V_{i,18}$	$-\Sigma_{i=1,6,21} P_i \cdot V_{i,18}$			(-1-Y _{HSRB,18})	(-1-Y _{HSRB,18})	$k_{M,HSRB} \frac{S_{VFA}}{K_{M,HSRB} + S_{VFA}} \cdot \frac{S_{SO4}}{K_{S,HSRB} + S_{SO4}} \cdot X_{HSRB} \cdot I_{AN} \cdot I_{P} \cdot I_{SO4} \cdot I_T$
19 Autotrophic uptake by ASRB				$-\Sigma_{i=1,2,4,21} C_{i,V,19}$	-1		$-\Sigma_{i=1,5,21} N_i \cdot V_{i,19}$	$-\Sigma_{i=1,6,21} P_i \cdot V_{i,19}$			(-1-Y _{ASRB,19})	(-1-Y _{ASRB,19})	$k_{M,ASRB} \frac{S_{SO4}}{K_{M,ASRB} + S_{SO4}} \cdot \frac{S_{CO2}}{K_{CO2,ASRB} + S_{CO2}} \cdot X_{ASRB} \cdot I_{AN} \cdot I_{P} \cdot I_{SO4} \cdot I_T$
20 Autotrophic uptake of H ₂ S by PPB				$-\Sigma_{i=1,2,4,21} C_{i,V,20}$			$-\Sigma_{i=1,5,21} N_i \cdot V_{i,20}$	$-\Sigma_{i=1,6,21} P_i \cdot V_{i,20}$			1	-1	$k_{M,S} \frac{S_{H2S}}{K_{M,S} + S_{H2S}} \cdot \frac{S_{CO2}}{K_{CO2} + S_{CO2}} \cdot X_{PPB} \cdot I_{AN} \cdot I_{AC} \cdot I_{P} \cdot I_{I} \cdot I_{O} \cdot I_{SO4} \cdot I_T$
21 Autotrophic uptake by microalgae				-1	Y _{Algae,S}		$-\Sigma_{i=1,5,21} N_i \cdot V_{i,21}$	$-\Sigma_{i=1,6,21} P_i \cdot V_{i,21}$					$k_{M,Algae} \frac{S_{CO2}}{K_{M,Algae} + S_{CO2}} \cdot X_{Algae} \cdot I_{AN} \cdot I_{P} \cdot I_T$
22 Heterotrophic uptake by microalgae			-1	$-\Sigma_{i=1,2,4,21} C_{i,V,22}$	(-1-Y _{Algae,H})		$-\Sigma_{i=1,5,21} N_i \cdot V_{i,22}$	$-\Sigma_{i=1,6,21} P_i \cdot V_{i,22}$					$k_{M,Algae,H} \frac{S_{VFA}}{K_{M,Algae,H} + S_{VFA}} \cdot \frac{S_{CO2}}{K_{CO2} + S_{CO2}} \cdot X_{Algae} \cdot I_{AN} \cdot I_{P} \cdot I_{I} \cdot I_T$
VFA's other than acetate (g COD m ⁻³)													Inhibition factors: $I_{AN} = \frac{K_{I,AN}}{K_{I,AN} + S_{AN}}$ $I_{AC} = \frac{S_{AC}}{K_{I,AC} + S_{AC}}$ $I_{P} = \frac{S_P}{K_{I,P} + S_P}$
Acetate (g COD m ⁻³)													$I_0 = \frac{K_{I,0}}{K_{I,0} + S_0}$ $I_{I1} = \frac{K_{I,I1}}{K_{I,I1} + S_{I1}}$
Inorganic carbon (f _{IC} (C m ⁻³))													$I_1 = \frac{K_{I,1}}{K_{I,1} + S_1}$ $I_{I1}^* = \frac{K_{I,1}^*}{K_{I,1}^* + S_{I1}^*}$
Hydrogen (g COD m ⁻³)													$I_{I1}^* = \frac{K_{I,1}^*}{K_{I,1}^* + S_{I1}^*}$ $I_{I1}^{**} = \frac{K_{I,1}^{**}}{K_{I,1}^{**} + S_{I1}^{**}}$
Oxygen (g O ₂ m ⁻³)													$I_{I1}^{**} = \frac{K_{I,1}^{**}}{K_{I,1}^{**} + S_{I1}^{**}}$
Inorganic nitrogen (g N m ⁻³)													$I_{I1}^{**} = \frac{K_{I,1}^{**}}{K_{I,1}^{**} + S_{I1}^{**}}$
Inorganic phosphorus (g P m ⁻³)													$I_{I1}^{**} = \frac{K_{I,1}^{**}}{K_{I,1}^{**} + S_{I1}^{**}}$
Biodegradable organic matter (g COD m ⁻³)													$I_{I1}^{**} = \frac{K_{I,1}^{**}}{K_{I,1}^{**} + S_{I1}^{**}}$
Soluble inerts (g COD m ⁻³)													$I_{I1}^{**} = \frac{K_{I,1}^{**}}{K_{I,1}^{**} + S_{I1}^{**}}$
S as sulphate (g S m ⁻³)													$I_{I1}^{**} = \frac{K_{I,1}^{**}}{K_{I,1}^{**} + S_{I1}^{**}}$
Soluble sulphates (g S m ⁻³)													$I_{I1}^{**} = \frac{K_{I,1}^{**}}{K_{I,1}^{**} + S_{I1}^{**}}$

Component →	i	12	13	14	15	16	17	18	19	20	21	Rate (g COD·m ⁻³ ·d ⁻¹)
j	Process ↓	X _{FM}	X _{FA}	X _{FI}	X _{FC}	X _{FD}	X _{FSB}	X _{ASB}	X _{AI}	X _C	X _I	
1	Hydrolysis									-1	f _{0,32}	$k_{HYD} X_C I_T$
2	Phototrophic acetate uptake by PPB	Y _{PPB}										$k_{PPB} \frac{S_{FA}}{K_{FA} + S_{FA}} X_{PPB} I_{FA} I_T I_{AI} I_T$
3	Phototrophic VFA uptake by PPB	Y _{PPB}										$k_{PPB} \frac{S_{VFA}}{K_{VFA} + S_{VFA}} X_{PPB} I_{VFA} I_T I_{AI} I_T$
4	VFA fermentation by PPB	Y _{PPB}										$k_{PPB} \frac{S_{VFA}}{K_{VFA} + S_{VFA}} X_{PPB} I_{VFA} I_T I_{AI} I_T$
5	Organics fermentation by PPB	Y _{PPB}										$k_{PPB} \frac{S_{ORG}}{K_{ORG} + S_{ORG}} X_{PPB} I_{ORG} I_T I_{AI} I_T$
6	Acetate uptake aerobically by PPB	Y _{PPB}										$k_{PPB} \frac{S_{FA}}{K_{FA} + S_{FA}} X_{PPB} I_{FA} I_T I_{AI} I_T$
7	VFA uptake aerobically by PPB	Y _{PPB}										$k_{PPB} \frac{S_{VFA}}{K_{VFA} + S_{VFA}} X_{PPB} I_{VFA} I_T I_{AI} I_T$
8	Organics uptake aerobically by PPB	Y _{PPB}										$k_{PPB} \frac{S_{ORG}}{K_{ORG} + S_{ORG}} X_{PPB} I_{ORG} I_T I_{AI} I_T$
9	Acetate uptake by aerobes		Y _{FA}									$k_{FA} \frac{S_{FA}}{K_{FA} + S_{FA}} X_{FA} I_T I_{AI} I_T$
10	VFA uptake by aerobes		Y _{VFA}									$k_{VFA} \frac{S_{VFA}}{K_{VFA} + S_{VFA}} X_{VFA} I_T I_{AI} I_T$
11	Organics uptake by aerobes		Y _{ORG}									$k_{ORG} \frac{S_{ORG}}{K_{ORG} + S_{ORG}} X_{ORG} I_T I_{AI} I_T$
12	Organics uptake by acidogens			Y _{FI}								$k_{FI} \frac{S_{FI}}{K_{FI} + S_{FI}} X_{FI} I_T I_{AI} I_T$
13	VFA uptake by acetogens				Y _{FC}							$k_{FC} \frac{S_{FC}}{K_{FC} + S_{FC}} X_{FC} I_T I_{AI} I_T$
14	Autotrophic uptake of H ₂ by PPB	Y _{PPB}										$k_{PPB} \frac{S_{H2}}{K_{H2} + S_{H2}} X_{PPB} I_{H2} I_T I_{AI} I_T$
15	Predation of aerobes by aerobic grazers		-1			Y _{FD}						$k_{FD} \frac{S_{FA}}{K_{FA} + S_{FA}} X_{FA} I_T I_{AI} I_T$
16	Predation of PPB by aerobic grazers	-1				Y _{FD}						$k_{FD} \frac{S_{VFA}}{K_{VFA} + S_{VFA}} X_{VFA} I_T I_{AI} I_T$
17	Acetate uptake by HSRB						Y _{HSRB}					$k_{HSRB} \frac{S_{FA}}{K_{FA} + S_{FA}} X_{HSRB} I_T I_{AI} I_T$
18	VFA uptake by HSRB						Y _{HSRB}					$k_{HSRB} \frac{S_{VFA}}{K_{VFA} + S_{VFA}} X_{HSRB} I_T I_{AI} I_T$
19	Autotrophic uptake by ASRB							Y _{ASRB}				$k_{ASRB} \frac{S_{H2}}{K_{H2} + S_{H2}} X_{ASRB} I_T I_{AI} I_T$
20	Autotrophic uptake of H ₂ S by PPB	Y _{PPB}										$k_{PPB} \frac{S_{H2S}}{K_{H2S} + S_{H2S}} X_{PPB} I_{H2S} I_T I_{AI} I_T$
21	Autotrophic uptake by microalgae							Y _{Algae,A}				$k_{Algae,A} \frac{S_{H2S}}{K_{H2S} + S_{H2S}} X_{Algae,A} I_T I_{AI} I_T$
22	Heterotrophic uptake by microalgae							Y _{Algae,H}				$k_{Algae,H} \frac{S_{ORG}}{K_{ORG} + S_{ORG}} X_{Algae,H} I_T I_{AI} I_T$
23	Decay of X _{FM}	-1								1		$k_{FM} X_{FM}$
24	Decay of X _{FA}		-1							1		$k_{FA} X_{FA}$
25	Decay of X _{FI}			-1						1		$k_{FI} X_{FI}$
26	Decay of X _{FC}				-1					1		$k_{FC} X_{FC}$
27	Decay of X _{FD}					-1				1		$k_{FD} X_{FD}$
28	Decay of X _{FSB}						-1			1		$k_{FSB} X_{FSB}$
29	Decay of X _{ASB}							-1		1		$k_{ASB} X_{ASB}$
30	Decay of X _{AI}								-1	1		$k_{AI} X_{AI}$

Inhibition factors:

$$I_A = \frac{K_{FA}}{K_{FA} + S_{FA}}$$

$$I_{VFA} = \frac{K_{VFA}}{K_{VFA} + S_{VFA}}$$

$$I_{ORG} = \frac{K_{ORG}}{K_{ORG} + S_{ORG}}$$

$$I_{H2} = \frac{K_{H2}}{K_{H2} + S_{H2}}$$

$$I_{H2S} = \frac{K_{H2S}}{K_{H2S} + S_{H2S}}$$

$$I_{AI} = \frac{K_{AI}}{K_{AI} + S_{AI}}$$

$$I_{AI}^* = \frac{K_{AI}^*}{K_{AI}^* + S_{AI}^*}$$

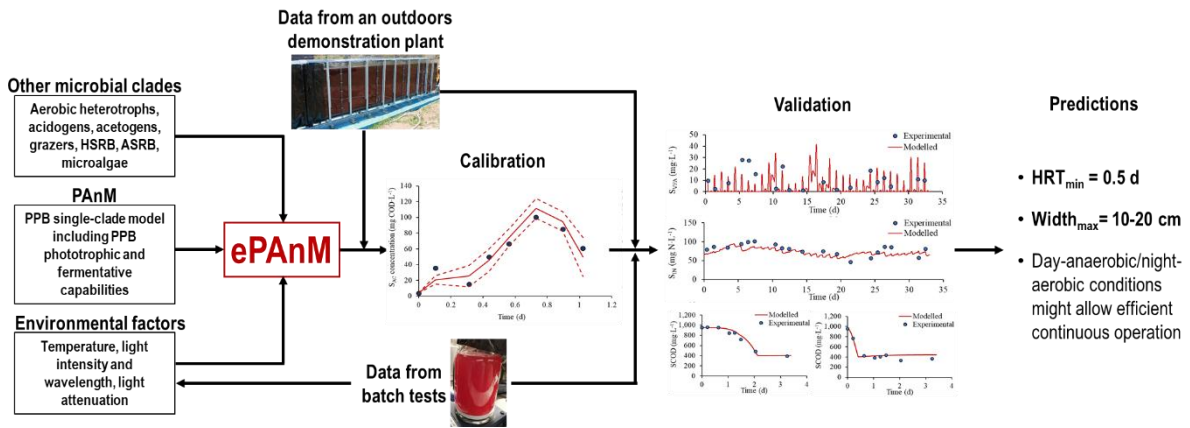
* See section 2.1.2

Table 2. Parameters calibrated to fit the experimental results from the cycle study carried out in the demonstration-scale flat plate PBR.

Symbol	Parameter	Value	Confidence interval	Units	Reference value ¹
Kinetic parameters related to PPB phototrophic uptake					
$k_{M,ac}$	Maximum photoheterotrophic S_{AC} uptake rate for X_{PB}	2.735	(1.709 -3.760)	mg COD·mg COD ⁻¹ ·d ⁻¹	2.4
$k_{M,vfa}$	Maximum photoheterotrophic S_{VFA} uptake rate for X_{PB}	1.680	(1.349-2.010)	mg COD·mg COD ⁻¹ ·d ⁻¹	1.4
K_{AC}	Half saturation constant for phototrophic S_{AC} uptake by X_{PB}	17.80	(16.83-18.77)	mg COD·L ⁻¹	20
K_{VFA}	Half saturation constant for phototrophic S_{VFA} uptake by X_{PB}	0.5	-	mg COD·L ⁻¹	0.5
Composition of biomass					
N_{XB}	Nitrogen content in biomass	0.0932	(0.067-0.1195)	mg N·mg COD ⁻¹	0.086
P_{XB}	Phosphorus content in biomass	0.0147	(0.002-0.027)	mg P·mg COD ⁻¹	0.015

1. From the PANM presented in Puyol et al. (2017).

Graphical abstract



Journal Pre-proof